Article

Current Biology

Mechanoregulation of basal body integrity during *Plasmodium* exflagellation

Graphical abstract

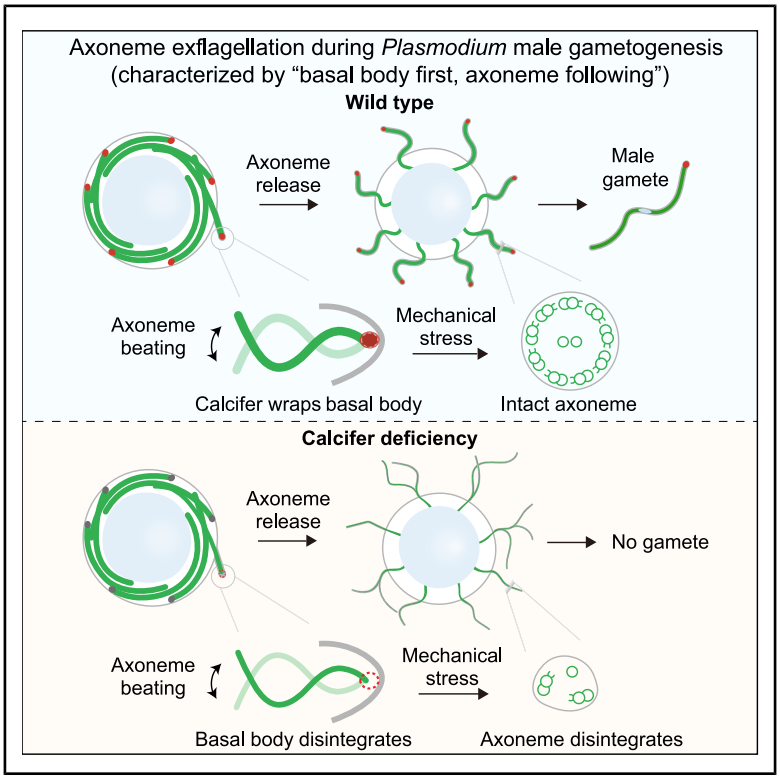

Highlights

- *Plasmodium* Calcifer is essential for axoneme release in male gametogenesis
- Calcifer translocates to the basal body after axoneme assembly
- Calcifer stabilizes the basal body under mechanical stress from axoneme beating
- Calcifer forms a sheath-like structure around the basal body

Authors

Jiepeng Guan, Yujiao Gong, Wenqi Liang, Huiting Cui, Jing Yuan

Correspondence

cuihuiting@xmu.edu.cn (H.C.), yuanjing@xmu.edu.cn (J.Y.)

In brief

How the structurally simplified basal body withstands extreme mechanical stress during *Plasmodium*'s unusually rapid axoneme release with basal body first is a puzzle. Guan et al. reveal that the *Plasmodium* Calcifer protein translocates to the basal body after axoneme assembly and stabilizes basal body integrity under the mechanical stress generated from axoneme beating.

Guan et al., 2026, Current Biology *36*, 1–17
May 4, 2026
https://doi.org/10.1016/j.cub.2026.03.068

CellPress

Current Biology

CellPress

Article

Mechanoregulation of basal body integrity during *Plasmodium* exflagellation

Jiepeng Guan,[1,2] Yujiao Gong,[1,2] Wenqi Liang,[1] Huiting Cui,[1,*] and Jing Yuan[1,3,*]
[1]State Key Laboratory of Cellular Stress Biology, School of Life Sciences, Faculty of Medicine and Life Sciences, Xiamen University, Xiamen 361102, Fujian, China
[2]These authors contributed equally
[3]Lead contact
*Correspondence: cuihuiting@xmu.edu.cn (H.C.), yuanjing@xmu.edu.cn (J.Y.)
https://doi.org/10.1016/j.cub.2026.03.068

SUMMARY

Constant mechanical stress challenges the structural integrity of cell systems. During malaria parasite transmission from mammal to mosquito, *Plasmodium* male gametogenesis features a unique axoneme release pattern characterized by basal body first, axoneme following. Substantial mechanical stress from axonemal beating threatens basal body integrity during axoneme exflagellation. However, how *Plasmodium* adapts to such mechanical stress and maintains the structural integrity of the basal body remains elusive. In this study, we identified a conserved *Plasmodium* protein, Calcifer, essential for male gamete formation and mosquito transmission of the parasite. Calcifer translocates to the basal body after axoneme assembly and persists during exflagellation, which is distinct from canonical basal body proteins. Parasites lacking Calcifer form intact axonemes but show rapid axoneme disintegration during exflagellation, a defect that can be rescued by inhibiting axoneme beating. *In vivo* and *in vitro* assays revealed that Calcifer directly stabilizes basal body integrity under mechanical forces generated by axoneme beating. Calcifer forms a wrapping structure around the basal body at the axoneme minus end, providing resistance to mechanical stress. Our findings elucidate a mechanical stabilization mechanism of the basal body that resists axoneme-beating-induced mechanical stress and reveal Calcifer as a key factor safeguarding basal body integrity during *Plasmodium* axoneme exflagellation.

INTRODUCTION

Malaria, an infectious disease caused by protozoan parasites *Plasmodium*, constitutes a global public health challenge, with 282 million cases and 610,000 deaths worldwide in 2024.[1] Beyond public health significance, *Plasmodium* is a model of highly divergent biology and evolves non-canonical cellular mechanisms to complete its life cycle, alternating between mammal hosts and female *Anopheles* mosquito vectors. A striking manifestation occurs during parasite transmission in the mosquito. In mammals, a small proportion of intraerythrocytic parasites differentiate sexually into female and male gametocytes, which are essential for malaria transmission to mosquitoes.[2] When a mosquito takes a blood meal, gametocytes are promptly activated and differentiate into fertile gametes in the midgut lumen, a process known as gametogenesis.[3] A female gametocyte produces one female gamete, whereas a male gametocyte develops into eight uniflagellated male gametes.[4,5] In the *Plasmodium* life cycle, the male gamete is the sole motile stage that possesses an axoneme. Driven by axoneme beating, a male gamete fertilizes a female gamete to form a zygote. Following further development into ookinetes, oocysts, and sporozoites within mosquitoes, the parasites in the mosquito salivary gland ultimately infect a vertebrate host, completing the malarial transmission.[5]

Male gametogenesis comprises the pre-exflagellation and exflagellation stages, lasting 12 to 15 min. During pre-exflagellation, three rounds of genome duplication occur without nuclear division, resulting in an octoploid nucleus.[6,7] Meanwhile, eight basal bodies are *de novo* assembled on the nuclear envelope and direct the assembly of eight axonemes in the cytoplasm.[4,8] Spindle-mediated chromosome segregation in the nucleus and basal body-directed axoneme formation in the cytoplasm are coordinated by a bipartite microtubule organization center (-MTOC) that spans the nuclear envelope.[9,10] Within this bipartite MTOC, the basal body on the cytoplasmic side serves as the nucleation template for the axoneme, while the spindle pole on the nuclear side provides the template for the spindle.[11–15] By the end of pre-exflagellation, each of the eight axonemes grows to approximately 14 μm and coils around the nucleus.[9,16] In the nucleus, each of the eight hemispindles captures one set of haploid chromosomes.[16–18] During the subsequent exflagellation stage, each mature axoneme beats vigorously in the cytoplasm and quickly releases from the gametocyte cell body with a haploid nucleus, yielding eight uniflagellate haploid male gametes.[19,20] Ultimately, each sperm-like male gamete contains an axoneme, a haploid nucleus, and a plasma membrane.[3,16,21]

Notably, *Plasmodium* displays a distinct axoneme release pattern characterized by a basal body first, followed by axoneme sequence during exflagellation. In canonical flagellum- or

Please cite this article in press as: Guan et al., Mechanoregulation of basal body integrity during *Plasmodium* exflagellation, Current Biology (2026), https://doi.org/10.1016/j.cub.2026.03.068

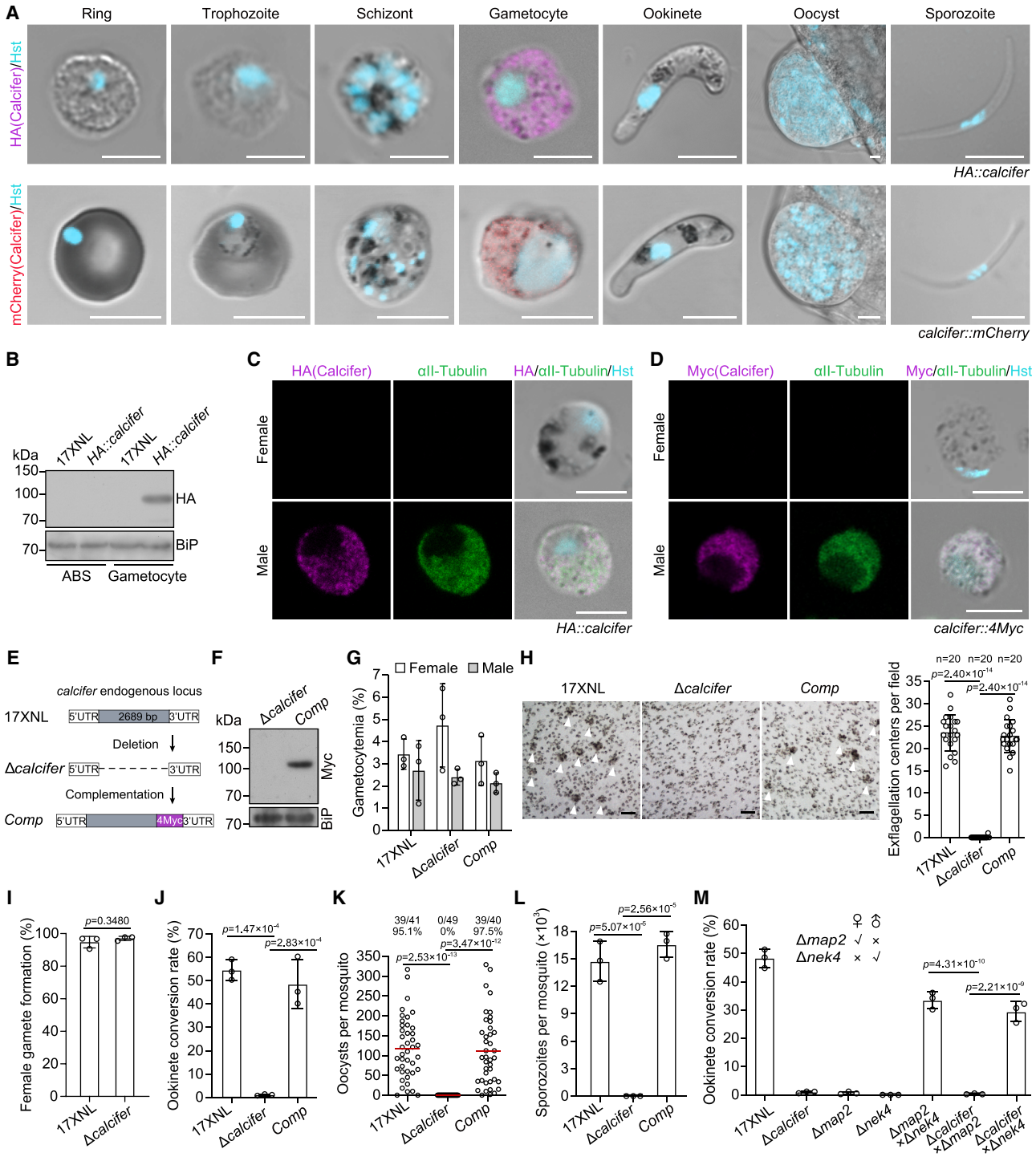

Figure 1. Calcifer is a male gametocyte protein essential for male gamete formation of *Plasmodium*

(A) Stage expression analysis of Calcifer during the life cycle of *P. yoelii*. Top: IFA of Calcifer in the *HA::calcifer* parasites in which the endogenous Calcifer was tagged with an HA in the N terminus. Bottom: live-cell imaging of Calcifer in the *calcifer::mCherry* parasites in which Calcifer was tagged with mCherry in the C terminus. Hst, Hoechst 33342. Scale bar, 5 μm. Three independent experiments.

(B) Immunoblot of Calcifer in the ABS and gametocyte of the *HA::calcifer* parasites. BiP, loading control. Three independent experiments.

(C) IFA of HA-tagged Calcifer and αII-tubulin (highly expressed in male gametocytes) in *HA::calcifer* gametocytes. Scale bars, 5 μm. Three independent experiments.

(D) IFA of 4Myc-tagged Calcifer and αII-tubulin in *calcifer::4Myc* gametocytes. Scale bars, 5 μm. Three independent experiments.

(legend continued on next page)

Please cite this article in press as: Guan et al., Mechanoregulation of basal body integrity during *Plasmodium* exflagellation, Current Biology (2026), https://doi.org/10.1016/j.cub.2026.03.068

cilium-containing cells, the basal body remains stationarily docked beneath the plasma membrane throughout axoneme assembly and beating.[22–25] By contrast, *Plasmodium* exhibits dynamic positioning of the basal body. Initially, basal bodies are anchored to the nuclear envelope to direct axoneme assembly; however, they become mobile during axoneme exflagellation.[9,26] Following active axoneme beating, the mechanical force generated thereby propels the basal body toward the cell periphery and further outward against the parasite plasma membrane to drive protrusion.[16] Both the vibration derived from axoneme beating and the shear force originating from the plasma membrane are presumed to exert significant mechanical stress on the basal body. Given the rapid rate of axoneme release, it is expected that the basal body is continuously exposed to such mechanical stress, which poses challenges to its structural integrity and functional stability.

The basal body constitutes a conserved structural component that orchestrates axoneme assembly. Comparative genomic analyses have revealed the absence of numerous conserved basal body component genes (RSP5, RSP7, RSP8, CEP164, and POC5) in *Plasmodium*,[27,28] indicating that their basal bodies may adopt a minimalistic structural organization. Consistent with these findings, neither early electron microscopy (EM) studies nor recent cryoelectron tomography (cryo-ET) analyses could detect signals corresponding to the cartwheel and spoke-core structural elements of the basal body in *Plasmodium*.[29,30] However, the conserved cartwheel assembly factor protein SAS6 exists in *Plasmodium*.[27,31] Furthermore, *Plasmodium* has lost the characteristic 9-fold symmetrical organizational arrangement typical of basal bodies. In addition, their axonemal microtubule formation involves a singlet-to-doublet microtubule transition,[8,29,30] which is distinct from the canonical microtubule triplet-to-doublet transition in most organisms.[23,32–34] Collectively, these observations suggest that *Plasmodium* has evolved a simplified basal body structure. In light of the apparent structural simplification, how the basal body adapts to mechanical stress and preserves its structural integrity during axoneme exflagellation remains elusive in *Plasmodium*.

In this study, we uncover a distinct *Plasmodium*-conserved protein, Calcifer, which is essential in axoneme exflagellation during male gametogenesis. Calcifer translocates to the basal body after axoneme assembly. Calcifer is not required for the axoneme assembly, which is distinct from the canonical roles of the basal body component proteins. During axoneme exflagellation, Calcifer functions as a stabilizing factor to resist axoneme-beating mechanical stress and safeguard basal body integrity. Our findings shed new light on how the eukaryotic cellular structure evolves to withstand extreme forces in the mechanostress-related motility process.

RESULTS

Calcifer is a *Plasmodium*-conserved protein essential for male gamete formation

The gene PY17X_1323900 encodes an uncharacterized *Plasmodium*-conserved protein (Figure S1). No identified domain or motif was detected in this protein. Previous studies revealed gametocyte-specific transcription of the gene orthologs in *P. falciparum*, *P. berghei*, and *P. yoelii*.[35–38] So far, the expression and function of this protein remain unknown. In this study, we named this protein PY17X_1323900 Calcifer and investigated its localization, function, and mechanism in *P. yoelii*. To investigate the stage expression and cellular localization of Calcifer during the life cycle of the parasite, we tagged the endogenous Calcifer with an HA epitope at the N terminus in *P. yoelii* 17XNL using CRISPR-Cas9, generating the line *HA::calcifer*. The *HA::calcifer* parasite developed normally in mice and mosquitoes, indicating that HA tagging does not affect protein function. Immunofluorescent assay (IFA) revealed that Calcifer was expressed in gametocyte cytoplasm (Figure 1A, top). No IFA signal was detected in asexual blood stages (ABSs), ookinetes, oocysts, and sporozoites. An immunoblot further confirmed the gametocyte-specific expression of Calcifer (Figure 1B). We also tagged the endogenous Calcifer with a red fluorescence protein, mCherry, at the C terminus, generating the line *calcifer::mCherry*. Live-cell imaging revealed that Calcifer::mCherry was only detected at the cytoplasm in gametocytes (Figure 1A, bottom), which is similar to HA::Calcifer. Staining *HA::calcifer* gametocytes with antibodies against αII-tubulin (highly expressed in male gametocytes[39]) and HA showed that Calcifer was exclusively expressed in male gametocytes (Figure 1C). To further validate this, we tagged Calcifer with a 4Myc at the C terminus and detected the male gametocyte-specific expression of Calcifer in the *calcifer::4Myc* parasite line (Figure 1D).

To investigate the function of Calcifer in the parasite, we deleted the genomic sequence (2,689 bp) of *calcifer* in the *P. yoelii* 17XNL (wild type) using CRISPR-Cas9, generating the mutant line Δ*calcifer* (Figure 1E). Deletion of *calcifer* did not

(E) Schematic showing the *calcifer* gene deletion and complementation. The coding sequence (2,689 bp) was deleted, generating the mutant line Δ*calcifer*. The *calcifer* gene fused with a 4Myc was introduced back, generating the complemented line *Comp*.
(F) Immunoblot of Calcifer expression in the *Comp* gametocytes. Three independent experiments.
(G) Male and female gametocyte formation in mice. Mean ± SEM from three mice in each group. Two independent experiments.
(H) *In vitro* EC formation of male gametocytes at 10 min post activation (mpa). ECs are marked with white arrows. Scale bars, 5 μm. Right: quantification of ECs in the hemocytometer under a light microscope. *n* is the number of fields counted. Mean ± SEM; one-way ANOVA with Tukey's multiple comparisons test. Three independent experiments.
(I) Female gamete formation assayed by P28 staining. P28 is a female gamete plasma membrane protein. Mean ± SEM from three independent experiments; two-sided *t* test.
(J) Ookinete development *in vitro*. Mean ± SEM from three independent experiments; one-way ANOVA with Tukey's multiple comparisons test.
(K) Midgut oocyst formation in mosquitoes at day 7 post blood feeding. Numbers at the top indicate the ratio of infected/total mosquitoes (x/y) and the infection prevalence (%). Red lines, mean values. One-way ANOVA with Tukey's multiple comparisons test. Three independent experiments.
(L) Salivary gland sporozoite formation in mosquitoes at day 14 post blood feeding. 20 infected mosquitoes were analyzed per group. Mean ± SEM from three independent experiments; one-way ANOVA with Tukey's multiple comparisons test.
(M) Ookinete development of the parasite after genetic cross between Δ*calcifer* and Δ*map2* (male-defect) or Δ*nek4* (female-defect) parasites. Mean ± SEM from three independent experiments; one-way ANOVA with Tukey's multiple comparisons test.

Please cite this article in press as: Guan et al., Mechanoregulation of basal body integrity during *Plasmodium* exflagellation, Current Biology (2026), https://doi.org/10.1016/j.cub.2026.03.068

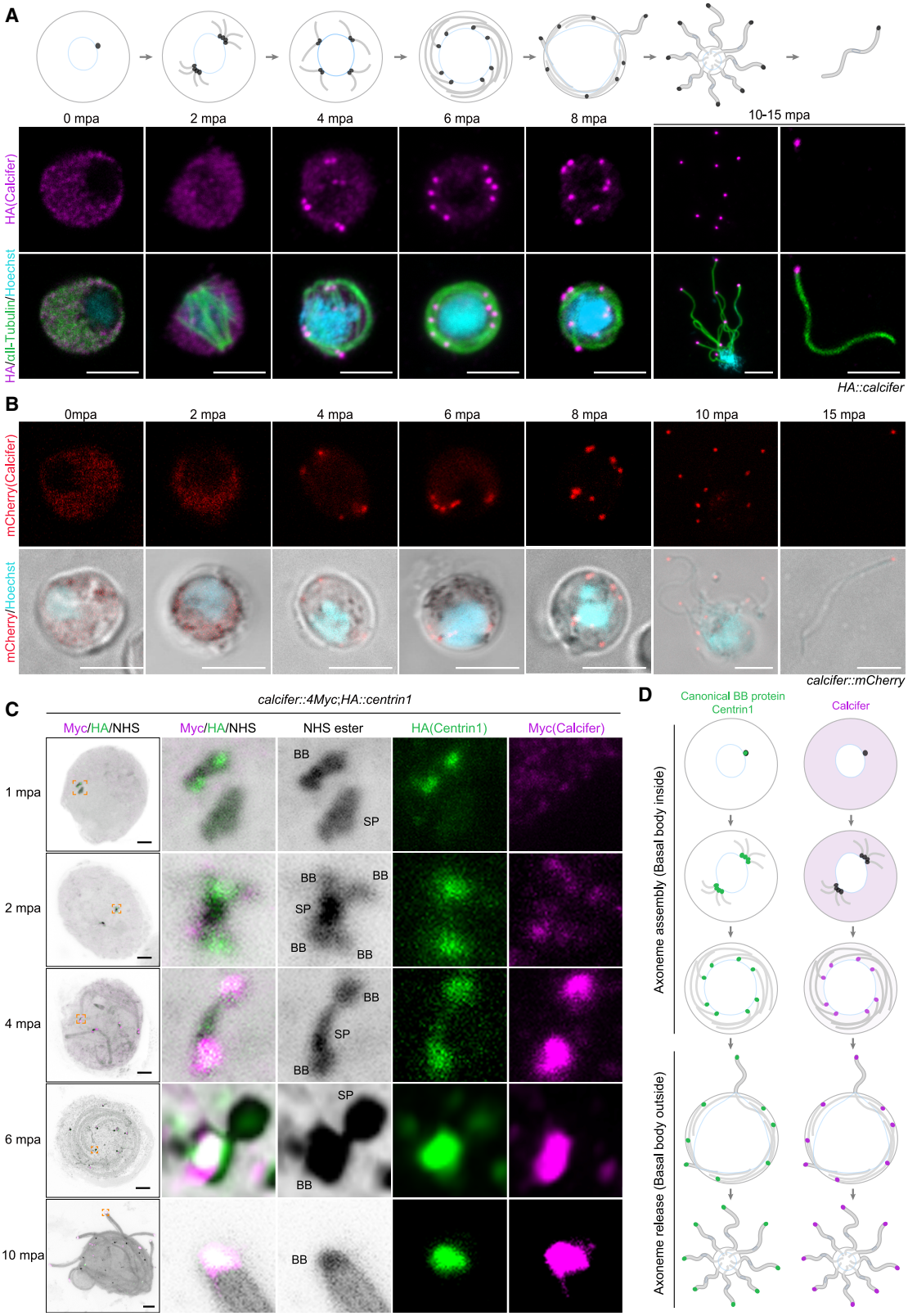

Figure 2. Calcifer translocates from the cytosol to the basal body after axoneme assembly

(A) IFA of HA-tagged Calcifer and αII-tubulin during male gametogenesis of the *HA::calcifer* parasite. Upper schematics show axoneme assembly and release processes in male gametogenesis. The basal body (black) and axoneme (gray) are indicated. Scale bars, 5 μm. Three independent experiments.

(legend continued on next page)

Please cite this article in press as: Guan et al., Mechanoregulation of basal body integrity during *Plasmodium* exflagellation, Current Biology (2026), https://doi.org/10.1016/j.cub.2026.03.068

affect male and female gametocyte development in mice (Figure 1G). We assessed parasite male gametogenesis by treating gametocytes with 100 μM xanthurenic acid at 22°C *in vitro*. Compared with 17XNL, Δ*calcifer* failed to form the exflagellation center (EC), a cell cluster of red blood cells caught by the exflagellated male gametocyte (Figure 1H), indicating defective male gamete formation. In contrast, Δ*calcifer* developed comparable female gametes *in vitro* as 17XNL (Figure 1I), which is consistent with the absence of Calcifer expression in female gametocytes. Δ*calcifer* failed to produce ookinetes *in vitro* (Figure 1J) and did not develop midgut oocysts or salivary gland sporozoites in the infected mosquitoes (Figures 1K and 1L), indicating a blockage of parasite transmission in mosquitoes.

To confirm that the Δ*calcifer* phenotype was due to the gene loss of *calcifer*, we introduced the deleted genomic sequence of *calcifer* tagged with 4Myc back to the locus in the Δ*calcifer*, generating the complemented line *Comp* (Figure 1E). An immunoblot detected the protein expression of Calcifer::4Myc in gametocytes of the *Comp* parasite (Figure 1F). The *Comp* parasite restored EC formation in activated male gametocytes (Figure 1H) and parasite transmission in mosquitoes (Figures 1J–1L). Last, we performed genetic crosses between Δ*calcifer* and Δ*map2* (male gamete-deficient) or Δ*nek4* (female gamete-deficient) parasites.[40,41] The cross between Δ*calcifer* and Δ*map2* failed to produce ookinetes, whereas the cross between Δ*calcifer* and Δ*nek4* generated a comparable number of ookinetes as the cross of Δ*map2* and Δ*nek4* (Figure 1M), confirming that Δ*calcifer* is only male gamete-deficient. These results demonstrate that Calcifer is essential for male gamete formation in the mosquito transmission of *P. yoelii*.

Calcifer translocates from the cytosol to the basal body after axoneme assembly

We investigated the localization dynamics of Calcifer during male gametogenesis of the *HA::calcifer* parasite. Before gametocyte activation, Calcifer and αII-tubulin were dispersed throughout the cytoplasm (Figure 2A). At 2 min post activation (mpa), the microtubules of nuclear spindles and cytoplasmic axonemes were assembled while Calcifer maintained cytosolic diffusion. From 4 to 6 mpa, Calcifer progressively translocated to eight discrete basal body foci likely associated with the nuclear envelope while the axoneme kept growing. After axoneme assembly at 7 to 8 mpa, Calcifer foci moved to the cell periphery. From 9 to 10 mpa, each of the eight axonemes exflagellated outward and were released from the gametocyte cell body, while Calcifer remained at the basal body during axoneme release (Figure 2A). Live-cell imaging of mCherry in the *calcifer::mCherry* parasite observed similar localization dynamics of Calcifer during male gametogenesis (Figure 2B).

Calcifer translocates from the cytosol to the basal body mainly after axoneme assembly. This localization dynamic of Calcifer is distinct from the canonical basal body proteins that localize to the basal body upon its assembly. We further investigated the localization dynamic difference between Calcifer and canonical basal body proteins. Two basal body proteins, Centrin1 and SAS4, were chosen.[42,43] Each of Centrin1 and SAS4 was endogenously tagged with HA or 6HA in the *calcifer::4Myc* parasite, generating two double-tagged parasite lines, *calcifer::4Myc;HA::centrin1* and *calcifer::4Myc;sas4::6HA*. We performed high-resolution ultrastructure expansion microscopy (U-ExM) to analyze the precise temporal-spatial relation between Calcifer and Centrin1 or SAS4 during male gametogenesis. At 1 and 2 mpa, one or two NHS-stained dense regions appeared (Figure 2C), referring to the amorphous bipartite MTOC (spindle pole and basal body) at the nuclear envelope.[44] Centrin1 was concentrated in the basal body, while Calcifer was dispersed in the cytoplasm (Figure 2C). At 4 mpa, Calcifer translocated to the basal bodies and co-localized with Centrin1. At 6 mpa, Calcifer was predominantly localized at the basal bodies and was not detected in the cytoplasm (Figure 2C). U-ExM analysis of Calcifer and SAS4 in the *calcifer::4Myc;sas4::6HA* line revealed similar localization dynamics of Calcifer during male gametogenesis (Figure S2A). To further confirm the basal body localization of Calcifer after axoneme assembly, we analyzed another protein, GCP3, which is a subunit of γ-tubulin ring complex (γ-TuRC) and marks both the basal body and spindle pole.[45] In the parasite line *calcifer::4Myc;gcp3::HA*, Calcifer was concentrated and accumulated at the basal body until 4 mpa, while GCP3 was localized in both the basal body and spindle pole from 1 mpa (Figure S2B). Together, these results demonstrate that Calcifer translocates from the cytosol to the basal body after axoneme assembly and localizes at the basal body during axoneme release (Figure 2D).

Intact cytoplasmic axoneme assembly in gametogenesis of a Calcifer-null parasite

We tested whether Calcifer regulates the axoneme assembly and/or axoneme release. IFA revealed that at 0 mpa, αII-tubulin was distributed throughout the cytosol of male gametocytes in both 17XNL and Δ*calcifer* (Figure 3A). At 6 mpa, axonemes were assembled and coiled around the enlarged nucleus in 17XNL and Δ*calcifer* (Figure 3B). Under U-ExM, axonemal microtubules exhibited a uniform diameter and consistent cytoplasmic organization, with no discernible differences between 17XNL and Δ*calcifer* (Figure 3C). We also stained gametocytes with an antibody targeting polyglutamylated tubulin (PolyE), a marker for axonemal microtubule in *Plasmodium* male gametocytes.[44,46] U-ExM analysis of PolyE also detected the intact axoneme structure at 6 mpa in both 17XNL and Δ*calcifer* (Figure 3D).

To further validate axoneme structural integrity, male gametocytes at 6 mpa were analyzed using transmission EM (TEM). In both 17XNL and Δ*calcifer* gametocytes, a large central nucleus was observed, which is indicative of nuclear genome replication (Figures 3E and 3F). Notably, longitudinal and cross-sectional TEM images revealed that the majority of axonemes in Δ*calcifer*

(B) Live-cell imaging of mCherry-tagged Calcifer during male gametogenesis of the *calcifer::mCherry* parasite. Scale bars, 5 μm. Three independent experiments.
(C) Ultrastructure expansion microscopy (U-ExM) of Calcifer and Centrin1 during male gametogenesis of the double-tagged line *calcifer::4Myc;HA::centrin1*. Centrin1 is a basal body protein. Parasites were stained with antibodies against HA and Myc and NHS ester dye. The basal body (BB) and spindle pole (SP) were densely labeled with NHS ester dye. Insets show enlargements of the boxed areas. Scale bars, 5 μm. Three independent experiments.
(D) Schematic showing different localization dynamics between canonical BB protein and Calcifer during axoneme assembly and release in male gametogenesis. See also Figure S2.

Please cite this article in press as: Guan et al., Mechanoregulation of basal body integrity during *Plasmodium* exflagellation, Current Biology (2026), https://doi.org/10.1016/j.cub.2026.03.068

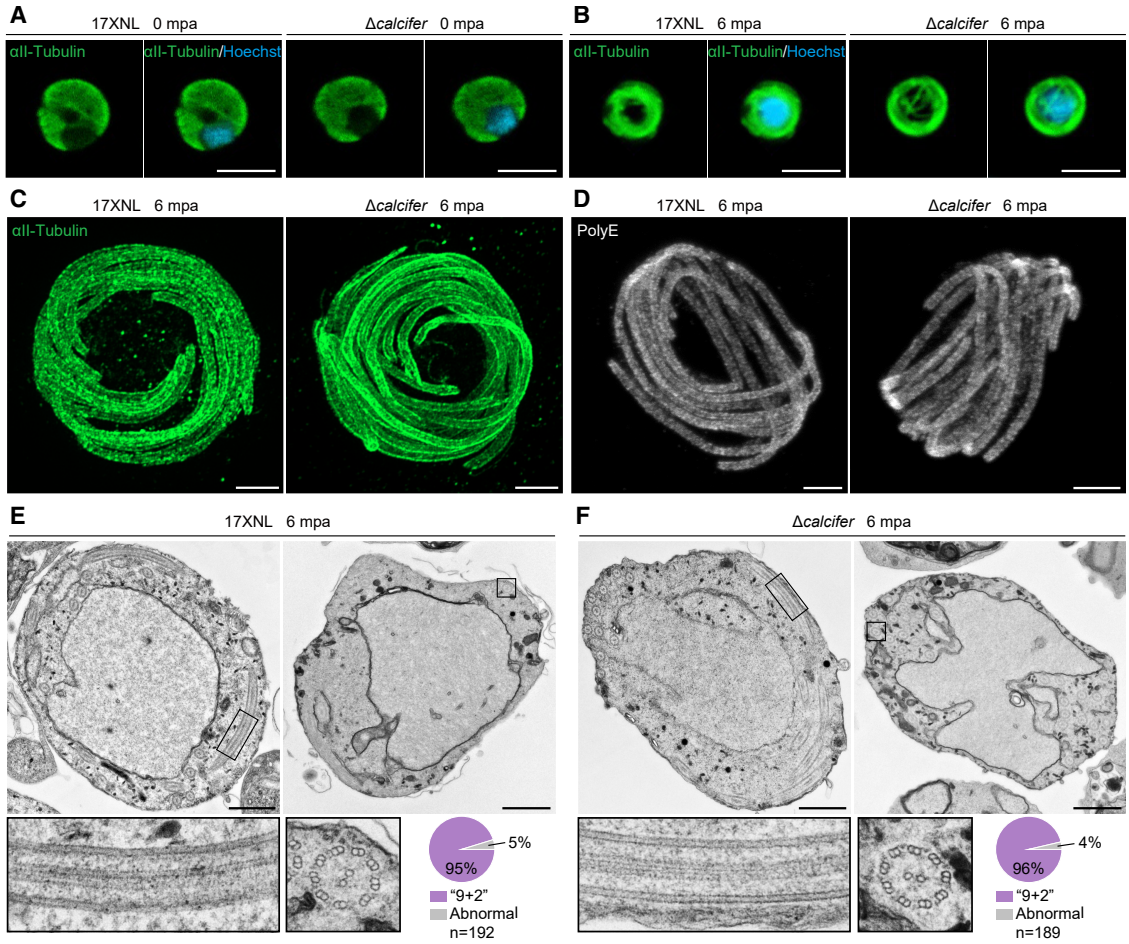

Figure 3. Intact axoneme assembly in gametogenesis of Calcifer-null parasite

(A and B) IFA of αII-tubulin in male gametocytes at 0 mpa (A) and 6 mpa (B). Scale bars, 5 μm. Representative of three independent experiments.

(C) U-ExM of αII-tubulin in male gametocytes at 6 mpa. Representative of three independent experiments. Scale bars, 5 μm.

(D) U-ExM of the PolyE in male gametocytes at 6 mpa. PolyE marks the mature B-tubule of the axonemal microtubule doublet. Representative of three independent experiments. Scale bars, 5 μm.

(E and F) TEM of axoneme architecture in male gametocytes at 6 mpa. Longitudinal sections (left) and cross sections (right) of axonemes are shown. The enclosed area (black box) was zoomed in. Pie charts show the quantification of axoneme (9 + 2 microtubules) in the parasites. *n* is the total number of intact and defective axoneme structures observed in each group. Three independent experiments with similar results. Scale bars, 1 μm.

See also Figure S3.

displayed the typical "9 + 2" microtubule arrangement (96%, *n* = 189 axonemes from 52 sections), which is indistinguishable from that in 17XNL (95%, 192 axonemes from 45 sections) (Figures 3E and 3F). These TEM results align with the U-ExM observations in Figures 3C and 3D. Previous results indicate that Calcifer translocates to the basal body after axoneme assembly. Consistent with this, axoneme assembly proceeds normally in the absence of Calcifer, implying that Calcifer exerts its functional role after axoneme assembly.

Axoneme disintegrates during exflagellation in the Calcifer-null parasite

After assembly, the axonemes actively beat and release from the cell body. Axonemal beating during early exflagellation was assessed using the *P. yoelii* reporter parasite line *DFsc7*, which expresses the axonemal dynein heavy-chain protein 1 (DHC1, PY17X_0418900) fused with GFP and displays GFP-labeled axonemes.[47] The *calcifer* gene was deleted in the *DFsc7*, generating the mutant line *DFsc7*;Δ*calcifer*. Live-cell imaging revealed that the axonemes in *DFsc7* exhibited vigorous beating for several minutes during release from 8 to 15 mpa, catching the surrounding cells to form ECs (Videos S1 and S2). In contrast, the axonemes in *DFsc7*;Δ*calcifer* only beat for dozens of seconds after release, with beating activity rapidly diminishing thereafter. Consequently, *DFsc7*;Δ*calcifer* failed to form an EC (Videos S3 and S4). Compared with the sustained axoneme beating in *DFsc7*, the Calcifer-null parasites could beat axonemes during early release but rapidly lost this capability.

We examined axoneme structural integrity during early exflagellation. Parasites generally initiate axoneme release at 8 mpa. We performed U-ExM and analyzed parasites at 9 mpa, enabling concurrent observation of axonemes in both

Please cite this article in press as: Guan et al., Mechanoregulation of basal body integrity during *Plasmodium* exflagellation, Current Biology (2026), https://doi.org/10.1016/j.cub.2026.03.068

CellPress

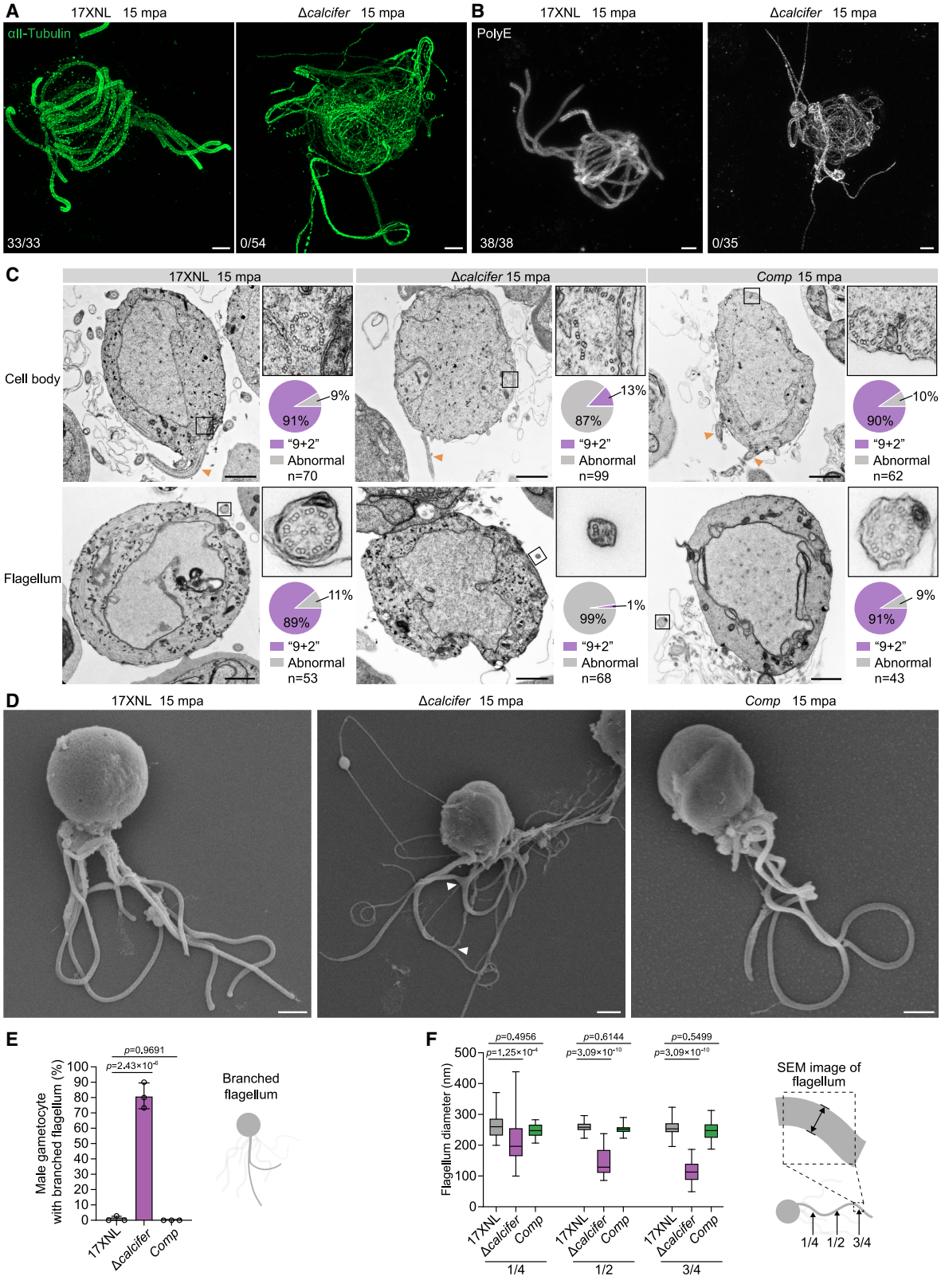

Figure 4. Axoneme disintegrates during exflagellation in the Calcifer-null parasite

(A and B) U-ExM of αII-tubulin (A) and PolyE (B) in male gametocytes at 15 mpa. Fractions (x/y) indicate gametocytes with intact axonemes/total cells analyzed. Three independent experiments. Scale bars, 5 μm.

(legend continued on next page)

Please cite this article in press as: Guan et al., Mechanoregulation of basal body integrity during *Plasmodium* exflagellation, Current Biology (2026), https://doi.org/10.1016/j.cub.2026.03.068

pre-release (non-exflagellating) and release (exflagellating) (Figures S3A and S3B). In 17XNL, axonemes maintained structural integrity in both non-exflagellating and exflagellating cells (Figure S3A). For Δ*calcifer* parasites, axonemes retained structural integrity in non-exflagellating cells but underwent disintegration in all exflagellating cells (n = 221) (Figures S3A and S3C). The specific disintegration of axonemes in exflagellating cells indicates this phenomenon occurs during the axoneme release process of Δ*calcifer*.

We further analyzed axoneme structural integrity during later exflagellation at 15 mpa. U-ExM revealed that the axonemal microtubules exhibited structural organization in both the cell body and flagellum of 17XNL (Figure 4A). However, 100% of axonemes in Δ*calcifer* were morphologically aberrant: they failed to maintain bundled structures, instead showing thin and branched filaments in both the cell body and flagellum (Figure 4A). We also stained Δ*calcifer* gametocytes with an anti-PolyE antibody and observed similar structural defects in axonemes (Figure 4B). Ultrastructural analysis via TEM revealed that axonemes in 17XNL displayed the 9 + 2 microtubule configuration in the cell body and flagellum (Figure 4C). In contrast, loss of Calcifer led to disintegration of the 9 + 2 axoneme structure in both the cell body and flagellum, resulting in scattered microtubule doublets and singlets in Δ*calcifer* (Figure 4C). In the complemented parasite line *Comp*, the 9 + 2 axoneme structure was restored to the level observed in 17XNL (Figure 4C). Aberrant exflagellation was additionally identified by scanning EM (SEM). 80% of Δ*calcifer* gametocytes developed branched flagella, a phenotype not detected in 17XNL (Figures 4D and 4E). Notably, this branched flagellum phenotype has not been reported in other gene mutants of *Plasmodium* parasites. Both 17XNL and *Comp* maintained a consistent flagellum diameter from proximal to distal ends, whereas the Δ*calcifer* flagella exhibited progressive tapering along this axis (Figures 4D and 4F). Separated microtubules likely protrude from the plasma membrane following axoneme disintegration, leading to flagellar branching and tapering. Therefore, Calcifer plays a critical role in maintaining axoneme structural integrity during exflagellation. The absence of Calcifer results in axoneme disintegration during early exflagellation, and consequently, axonemes in Calcifer-null parasites lose the beating ability required for further release.

Calcifer stabilizes basal body integrity under axoneme-beating-generated mechanical force

During axoneme release, the basal body orients outward toward the plasma membrane and encounters substantial shear forces induced by axoneme beating. It was reasoned that the basal body must resist these mechanical forces and maintain its structural integrity. Calcifer incorporates stably into the basal body after axoneme assembly, and its absence leads to axoneme disintegration during exflagellation. Based on these facts, we hypothesized that Calcifer directly contributes to stabilizing the structure of the basal body and the axoneme minus end. To examine basal body integrity in Calcifer-null parasites during exflagellation, we deleted the *calcifer* gene in three parasite lines with tagged basal body proteins (*HA::centrin1*, *sas4::6HA*, and *gcp3::4Myc*), obtaining three mutant clones *HA::centrin1*;Δ*calcifer*, *sas4::6HA*;Δ*calcifer*, and *gcp3::4Myc*;Δ*calcifer* (Figures 5A–5C). U-ExM analysis at 10 mpa showed that, in contrast to the parent parasites, these three proteins (Centrin1, SAS4, and GCP3) completely lost their basal body localization at the axoneme minus end in Calcifer-null parasites during exflagellation (Figures 5A–5D). These *in vivo* results demonstrated that the structural integrity of the basal body is disrupted during axoneme release in Calcifer-null parasites.

To determine whether the structural integrity of the basal body is compromised by the mechanical force generated by axoneme beating, we developed an *in vitro* vortex assay designed to simulate vibration-induced mechanical stress (Figure S4A). The *HA::calcifer* gametocytes at 6 mpa were treated with the detergent sodium deoxycholate (SDC) for lysis, allowing the release of intact axonemes (Figure S4B). U-ExM confirmed that Calcifer localizes to the basal body at the axoneme minus end (Figure S4C, left), indicating that SDC treatment did not impair the structural integrity of the basal body at the axoneme minus end. Furthermore, 100% of axonemes retained intact minus ends, whereas 19% exhibited bifurcation at the plus end (Figures S4C and S4D), suggesting that the axoneme plus end is structurally less stable than the minus end. These isolated *HA::calcifer* axonemes were then exposed to vortexing at 3,000 rpm for 1 min. After vortexing, 92% of axonemes maintained basal body integrity at the minus end, while 90% showed disintegration at the plus end (Figures S4C and S4D). These results indicated that the basal body exhibits structural stability under mechanical stress generated by *in vitro* vortexing.

Using this *in vitro* vortex assay, we analyzed the basal bodies and axonemes from Calcifer-null parasites. Before vortexing, the axonemes from both *sas4::6HA* and *sas4::6HA*;Δ*calcifer* parasites displayed SAS4 localization at the basal body situated at the minus end (Figure 5E). After vortexing, SAS4 remained concentrated in the basal body at the *sas4::6HA* axoneme minus end; however, such concentration was absent at the *sas4::6HA*;Δ*calcifer* axoneme minus end (Figures 5E and 5F). Additionally, *sas4::6HA*;Δ*calcifer* axonemes exhibited bifurcation at both plus and minus ends (Figures 5E and 5F), which is indicative of axoneme disintegration at both ends. We further analyzed the basal bodies and axonemes from *gcp3::4Myc* and *gcp3::4Myc*;Δ*calcifer* parasites. Consistently, the GCP3-labeled

(C) TEM of axoneme architecture in cell body (top) and flagellum (bottom) of male gametocytes at 15 mpa. The orange arrow indicates the exflagellating axonemes. The enclosed area (black box) was zoomed in. Pie charts show the quantification of axonemes with 9 + 2 microtubules. n is the number of axoneme structures analyzed in each group. Three independent experiments with similar results. Scale bars, 1 μm.
(D) SEM of exflagellating male gametocytes at 15 mpa. Branched flagella are marked with white arrows. Scale bars, 1 μm. Three independent experiments.
(E) Quantification of male gametocytes with branched flagella in (D). Mean ± SEM from three independent experiments; one-way ANOVA with Tukey's multiple comparisons test.
(F) Quantification of diameter from proximal to distal ends (1/4, 1/2, and 3/4 length) of axoneme in (D). Mean ± SEM from three independent experiments; one-way ANOVA with Tukey's multiple comparisons test.
See also Figure S3 and Videos S1, S2, S3, and S4.

Please cite this article in press as: Guan et al., Mechanoregulation of basal body integrity during *Plasmodium* exflagellation, Current Biology (2026), https://doi.org/10.1016/j.cub.2026.03.068

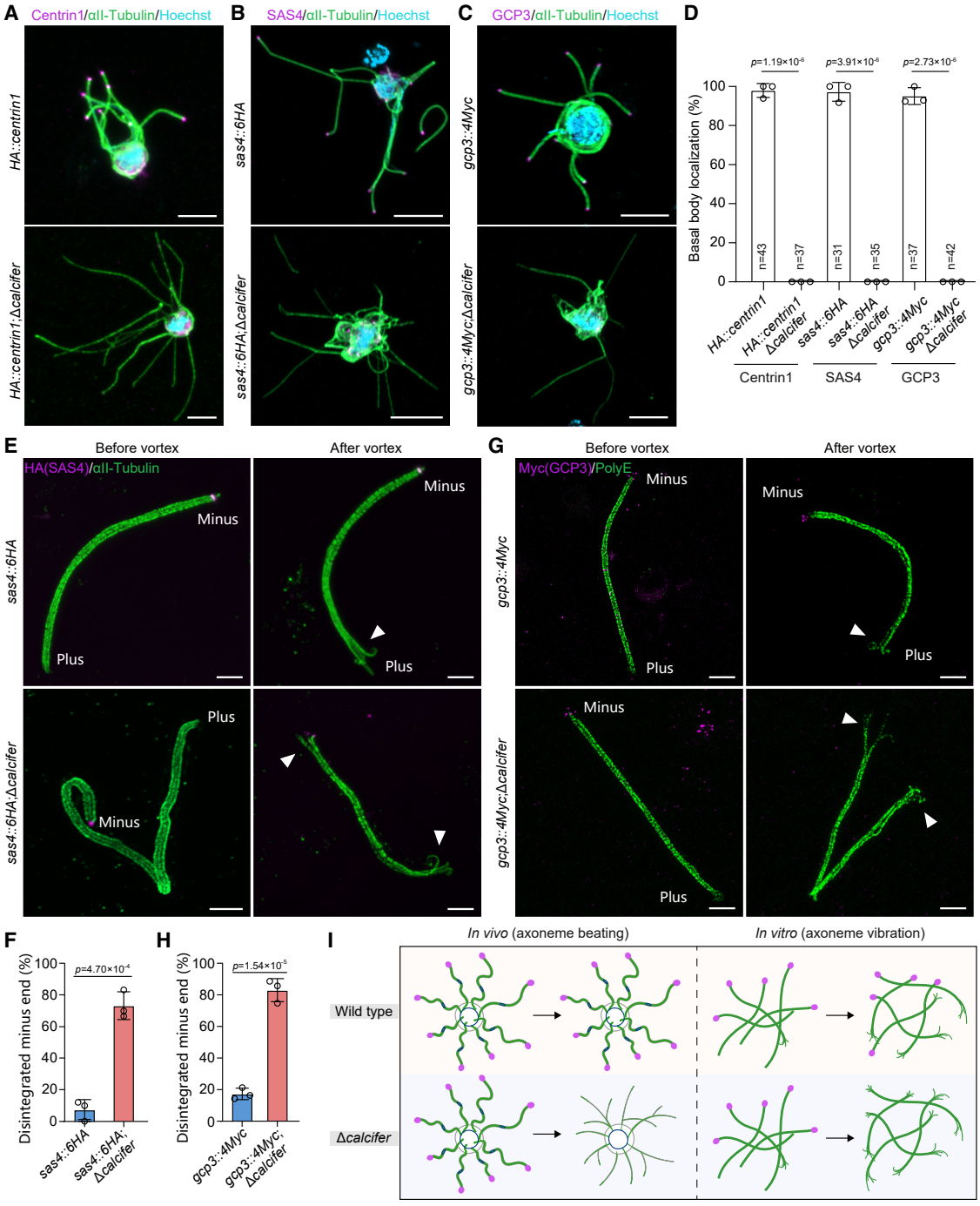

Figure 5. Calcifer stabilizes BB integrity under axoneme-beating-generated mechanical force

(A–C) IFA of αII-tubulin and three BB markers, HA-tagged Centrin1 (A), 6HA-tagged SAS4 (B), and 4Myc-tagged GCP3 (C), during axoneme exflagellation in gametocytes at 10 mpa for the indicated parasite lines. Scale bars, 5 μm. Three independent experiments.

(D) Quantification of the BB localization retention for the BB markers in (A)–(C). *n* is the number of basal bodies analyzed. Mean ± SEM; two-sided *t* test.

(E) U-ExM of SAS4 in axonemes after *in vitro* vortex simulating vibration-induced mechanical stress. Intact axonemes in *sas4::6HA* and *sas4::6HA*;Δ*calcifer* parasites were isolated from gametocytes at 6 mpa and exposed to vortexing at 3,000 rpm for 1 min. Axonemes were analyzed before and after vortexing. SAS4 signal marks the BB at the minus end of axonemes; white arrows indicate disintegrated ends. Scale bars, 5 μm.

(F) Quantification of disintegrated minus ends of axonemes after vortexing in (E). Mean ± SEM from three independent experiments; two-sided *t* test.

(G) U-ExM of GCP3 in axonemes after *in vitro* vortexing for *gcp3::4Myc* and *gcp3::4Myc*;Δ*calcifer* parasites. GCP3 signal marks the BB at the minus end of axonemes; white arrows indicate the disintegrated ends. Scale bars, 5 μm.

(legend continued on next page)

Please cite this article in press as: Guan et al., Mechanoregulation of basal body integrity during *Plasmodium* exflagellation, Current Biology (2026), https://doi.org/10.1016/j.cub.2026.03.068

basal body at the minus end disintegrated in Calcifer-null axonemes under vortex-induced mechanical stress (Figures 5G and 5H). These *in vitro* results demonstrate that Calcifer-null basal bodies are vulnerable to vortex-generated mechanical force, leading to basal body disintegration and subsequent breakdown of the axoneme minus end (Figure 5I).

Collectively, these *in vivo* and *in vitro* results confirm that the structural integrity of the basal body is compromised by mechanical forces derived from either beating or vortexing, and Calcifer could stabilize the basal body to resist damage induced by such mechanical forces.

Inhibition of axoneme beating rescues axoneme disintegration in the Calcifer-null parasite

We hypothesized that inhibiting axoneme beating during its release would prevent the generation of the mechanical forces required to trigger basal body disintegration in the Calcifer-null parasite. To further validate that Calcifer-dependent structural integrity of the basal body is compromised by mechanical force, we aimed to suppress axoneme beating during male gametogenesis. Axoneme beating relies on the motor activity of the axonemal dynein complex, where the dynein heavy-chain (DHC) subunit provides the motor force.[48] DHC1 (PY17X_0418900) encodes a putative axonemal DHC. Our previous studies demonstrated that DHC1 is specifically expressed in male gametocytes and localized to the axoneme of *P. yoelii*[47]; however, its functional role in axoneme beating remains unvalidated in *Plasmodium*. We deleted the N-terminal coding sequence (1,456 bp) of *dhc1* in 17XNL, generating the mutant line Δ*dhc1* (Figure S5A). Δ*dhc1* developed comparable levels of male and female gametocytes in mice relative to 17XNL (Figure S5B). Deletion of *dhc1* did not impact axoneme assembly in male gametocytes at 8 mpa (Figure S5C) or initial axoneme release at 15 mpa (Figures S5D and S5E). However, it completely abolished EC formation (Figure S5F). Consistently, Δ*dhc1* failed to develop midgut oocysts and salivary gland sporozoites in infected mosquitoes (Figures S5G and S5H). We further deleted the *dhc1* gene in the parasite line *calcifer::mCherry*, and the resulting mutant clone *calcifer::mCherry*;Δ*dhc1* displayed phenotypes consistent with Δ*dhc1* (Figures S5I and S5J). Notably, loss of DHC1 did not affect the basal body localization of Calcifer during axoneme release (Figure S5K). Live-cell imaging revealed weak axoneme beating after release in Δ*dhc1*, which is in stark contrast to the vigorous and sustained axoneme beating in *calcifer::mCherry* (Figure 6A; Videos S5 and S6). These results demonstrate that DHC1 specifically drives axoneme beating following its initial release from the cell body. DHC1 deficiency does not compromise basal body and axoneme integrity but impairs axoneme beating capacity after release.

Next, we investigated whether inhibiting axoneme beating could mitigate basal body and axoneme disintegration during exflagellation of Calcifer-null parasites. The *dhc1* gene was deleted in Δ*calcifer*, generating a double-gene-mutant clone Δ*calcifer*;Δ*dhc1*. U-ExM of axonemes stained with αII-tubulin antibody revealed that DHC1 deficiency alone did not alter axoneme structural integrity during exflagellation in Δ*dhc1* at 15 mpa (Figure 6B, third image), aligning with IFA and SEM results for Δ*dhc1* in Figure S6. Notably, DHC1 deficiency mitigated axoneme structural defects in Calcifer-null parasites during exflagellation at 15 mpa (Figure 6B, fourth image for Δ*calcifer*;Δ*dhc1*). In contrast to the thin and branched axonemes in Δ*calcifer*, most axonemes in Δ*calcifer*;Δ*dhc1* exhibited a thick and bundled morphology. Quantitative analysis revealed that 0% of male gametocytes in Δ*calcifer* (n = 64) had intact axonemes, whereas 92% of those in Δ*calcifer*;Δ*dhc1* (n = 71) did (Figure 6C).

TEM ultrastructural analysis of gametocytes at 15 mpa showed that the axonemes in Δ*dhc1* displayed the 9 + 2 microtubule arrangement in both cell body and flagellum, resembling those in 17XNL (Figure 6D). In contrast to the defective microtubule arrangement of axonemes in Δ*calcifer*, Δ*calcifer*;Δ*dhc1* restored the 9 + 2 microtubule arrangement of axonemes in both the cell body and flagellum (Figure 6D). The proportion of the 9 + 2 axonemes was 11% in the cell body (n = 221) and 0% in the flagellum (n = 52) of Δ*calcifer*, whereas it reached 94% in the cell body (n = 205) and 96% in the flagellum (n = 49) of Δ*calcifer*;Δ*dhc1* (Figures 6E and 6F). These results confirm that axoneme structure disintegration in Calcifer-null parasites is caused by axoneme beating during exflagellation. Consequently, inhibition of axoneme beating via *dhc1* gene deletion preserves axoneme structural integrity in Calcifer-null parasites. The rescue of axoneme disintegration by inhibition of axoneme beating further validates that the disintegration of basal bodies in Calcifer-null parasites is induced by mechanical forces generated by axoneme beating during exflagellation.

Calcifer wraps the basal body at the axoneme minus end

Next, we investigated the more precise localization of Calcifer within the basal body structure at the minus end of the axoneme. We performed U-ExM to analyze the spatial relationship between Calcifer and three basal body proteins (Centrin1, SAS4, and GCP3). The cartwheel at the inner core structure of the basal body consists of a central hub and nine radiating spokes, and Centrin1 is a cartwheel protein.[10] Encircling the cartwheel, SAS4 serves as a linker between the radiating spokes and peripheral microtubules.[49] GCP3 is a component protein of the γ-TuRC complex localized at the proximal end of peripheral microtubules.[50] The *calcifer::4Myc*;*HA::centrin1* gametocytes at 10 mpa were stained with anti-HA and anti-Myc antibodies, followed by U-ExM. Three-dimensional (3D) surface topology reconstruction of fluorescence signals revealed that Calcifer fully encompassed Centrin1 and exhibited a larger signal area than Centrin1 (Figure 7A). To eliminate potential discrepancies in fluorescence signals arising from secondary antibody-conjugated fluorophores, we swapped the fluorophores in secondary antibodies and stained the *calcifer::4Myc*;*HA::centrin1* gametocytes. U-ExM imaging confirmed that Calcifer still displayed a significantly larger signal area compared with Centrin1

(H) Quantification of disintegrated minus ends of axonemes after vortexing in (G). Mean ± SEM from three independent experiments; two-sided t test.
(I) Schematic of the BB (purple) and axoneme (green) integrity for the Calcifer-null parasite under the mechanical force generated by axoneme beating (*in vivo*) and axoneme vibration (*in vitro*).
See also Figure S4.

Please cite this article in press as: Guan et al., Mechanoregulation of basal body integrity during *Plasmodium* exflagellation, Current Biology (2026), https://doi.org/10.1016/j.cub.2026.03.068

CellPress

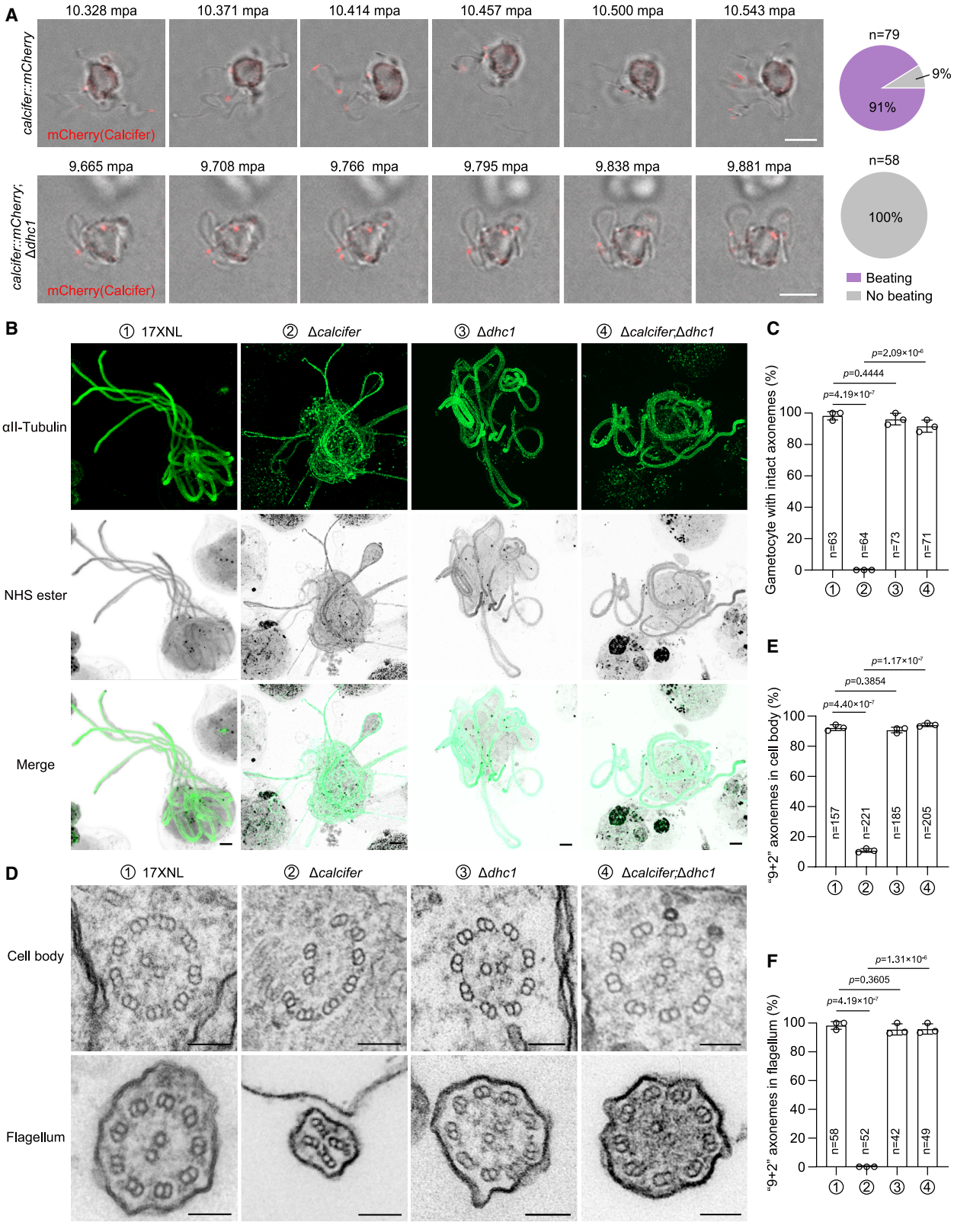

(legend on next page)

Please cite this article in press as: Guan et al., Mechanoregulation of basal body integrity during *Plasmodium* exflagellation, Current Biology (2026), https://doi.org/10.1016/j.cub.2026.03.068

(Figure 7B). Consistently, the signal area of Calcifer was significantly larger than that of SAS4 in the *calcifer::4Myc*;*sas4::6HA* parasites (Figures 7C and 7D) and than that of GCP3 in the *calcifer::4Myc*;*gcp3::HA* parasites (Figures 7E and 7F).

As a control, we validated the spatial relationship between SAS4 and GCP3 within the basal body. A double-tagged line, *gcp3::HA*;*sas4::4Myc* was generated, where endogenous GCP3 was tagged with HA and SAS4 was tagged with 4Myc. U-ExM showed that GCP3 largely overlapped with SAS4, and no significant difference in signal area was observed between the two proteins (Figures S6A and S6B). Since the spatial localization relationship between GCP3 and SAS4 is conserved in the basal body across eukaryotes,[51] this observation reinforces the reliability of our imaging-based protein localization analysis. Furthermore, we examined the relationship of Calcifer with axonemal microtubules in the *HA::calcifer* parasites. Calcifer signals consistently encompassed tubulin signals in the basal body at the axoneme minus end (Figures S6C and S6D). These results collectively suggest that Calcifer forms a sheath-like structure around the basal body at the axoneme minus end (Figure S6E).

DISCUSSION

This study identifies Calcifer, a *Plasmodium*-conserved protein, as a key regulator of basal body mechanical stability and integrity during male gametogenesis with rapid beating and release of the axoneme (Figure 7G). Canonical basal body proteins function primarily in nucleation, anchorage, and early assembly of axoneme microtubules. Distinct from the canonical basal body protein, Calcifer executes a specialized role in maintaining the mechanical stability of the basal body to counteract mechanical stress induced by rapid and constant axoneme beating. This unique function is tightly coupled to its spatiotemporal localization: Calcifer is not associated with the basal body during axoneme assembly but translocates to this structure after assembly, coinciding with the onset of axoneme beating—a timing that aligns with its role in maintaining mechanical stability rather than structural biogenesis.

The maintenance of basal body mechanical stability via basal body-localized proteins during axoneme beating is a rare phenomenon in eukaryotes. While axonemes beat in most flagellum- or cilium-containing cells, the basal body remains stationarily docked beneath the plasma membrane via the distal appendages and cortical cytoskeleton.[52–56] This docking ensures that the basal body acts as a stable platform that could buffer and resist the mechanical stress from axoneme bending or beating. In *Plasmodium* gametocytes, after cytoplasmic assembly, mature axonemes beat vigorously and quickly to release from the cell body at a speed (294–1,254 μm/h) that is orders of magnitude faster than axoneme outgrowth in model organisms (e.g., 9–24 μm/h in *Chlamydomonas reinhardtii*, 3.6 μm/h in *Trypanosoma brucei*, 0.6 μm/h in mouse sperm, and 0.1–2.6 μm/h in ciliated mammalian cells).[24,57–59] Notably, *Plasmodium* axonemes are released from the gametocyte with their minus ends leading, displaying a unique pattern characterized by a basal body first, followed by axoneme. When the basal bodies encounter the gametocyte plasma membrane, substantial mechanical forces derived from axoneme beating are required for successful release. This interaction creates additional membrane-derived mechanical resistance to the basal body. Compounding these challenges, *Plasmodium* has evolved a simplified basal body structure. The characteristic 9-fold symmetrical structures of cartwheels and spokes have not been detected in the basal body of *Plasmodium*.[30] Additionally, *Plasmodium* basal bodies lack the canonical rigid triplet microtubules but instead consist of singlet microtubules for axonemal doublet microtubule formation, which are thought to provide less structural reinforcement for the mechanical stability of the basal body and axoneme. Together, these features impose extraordinary mechanical stress on the structurally simplified basal body at the axoneme minus end during *Plasmodium* exflagellation. Our data demonstrate that Calcifer acts specifically at the basal body to maintain the mechanical stability of the basal body and thus the 9 + 2 microtubule structure of the axoneme. Nevertheless, the causal sequence of structural failure is inferred rather than directly visualized. It remains formally unclear whether structural disassembly initiates within the basal body core and secondarily affects the axoneme minus end, or whether destabilization of the axoneme minus end under force leads to subsequent loss of basal body marker localization. This localization-specific mechanism is particularly notable given the unique structural and mechanical features of *Plasmodium* exflagellation. In addition, our findings suggest that Calcifer has evolved to compensate for these structural limitations by forming a protective wrapping structure around the basal body, thereby enhancing its mechanical stability.

Phylogenetic analysis showed distribution of the homologous proteins of Calcifer in two other Apicomplexa parasites, *Hepatocystis* and *Haemoproteus*, but this is absent in conventional cilium- or flagellum-possessing organisms. *Hepatocystis* and *Haemoproteus* are close relatives of the *Plasmodium* parasites.[60,61] Notably, both *Hepatocystis* and *Haemoproteus* share key features with *Plasmodium* in male gametogenesis during the insect vector transmission of parasites, including axoneme

Figure 6. Inhibition of axoneme beating rescues axoneme disintegration in the Calcifer-null parasite

(A) Live-cell imaging of axoneme beating during exflagellation for *calcifer::mCherry* and *calcifer::mCherry*;Δ*dhc1* gametocytes. Axoneme beating during release was recorded for 13 s. MCherry signal indicates the BB. Scale bars, 5 μm. Pie charts quantify the proportion of male gametocytes with axoneme constant beating. *n* is the number of cells analyzed. Three independent experiments.

(B) U-ExM of axoneme architecture during exflagellation at 15 mpa. Parasites were stained with anti-αII-tubulin antibody and NHS ester. Δ*calcifer* and Δ*dhc1* are single-gene mutant lines, while Δ*calcifer*;Δ*dhc1* is a double-gene mutant line. Scale bars, 5 μm.

(C) Quantification of gametocytes with intact axonemes in (B). *n* is the number of cells analyzed. Mean ± SEM from three independent experiments; one-way ANOVA with Tukey's multiple comparisons test.

(D) TEM of axoneme architecture during exflagellation at 15 mpa. Scale bars, 100 nm.

(E and F) Quantification of 9 + 2 axonemes in the cell body (E) and flagellum (F). *n* is the number of axonemes analyzed. Mean ± SEM from three independent experiments; one-way ANOVA with Tukey's multiple comparisons test.

See also Figure S5 and Videos S5 and S6.

Please cite this article in press as: Guan et al., Mechanoregulation of basal body integrity during *Plasmodium* exflagellation, Current Biology (2026), https://doi.org/10.1016/j.cub.2026.03.068

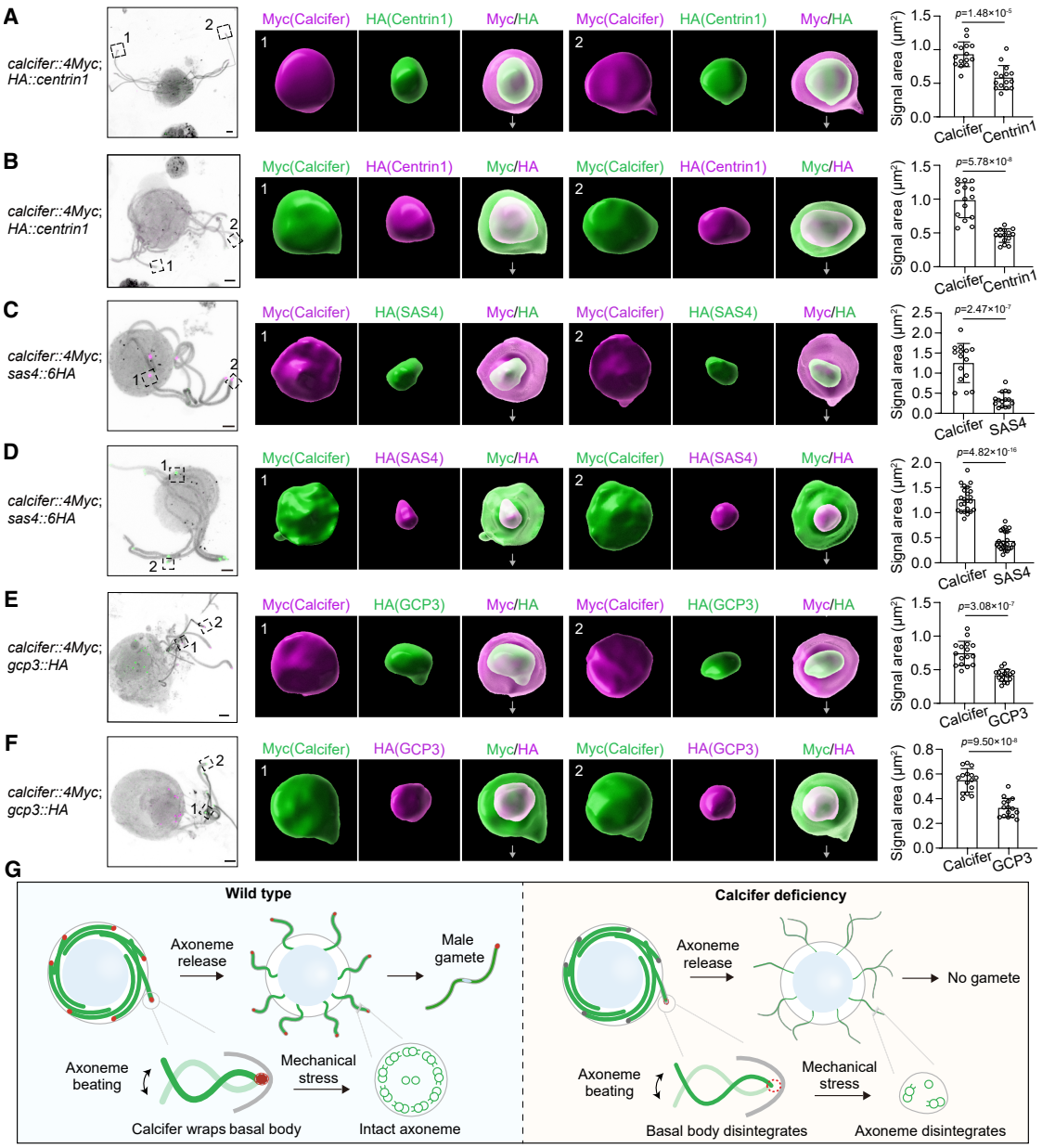

Figure 7. Calcifer wraps the BB at the axoneme minus end

(A, C, and E) U-ExM analysis of relative spatial localization between Calcifer and three BB markers, Centrin1 (A), SAS4 (C), and GCP3 (E), during axoneme exflagellation for the indicated parasite lines. Left: 2D projection images of male gametocytes at 10 mpa stained with the indicated primary antibodies (detected by anti-mouse-555 and anti-rabbit-488 secondary antibodies) and NHS ester. Scale bars, 5 μm. Middle: 3D surface topology reconstruction. Two boxed areas were zoomed in. White arrows show the axoneme direction. Right: quantification of fluorescence signal area for proteins. Mean ± SEM from three independent experiments; two-sided *t* test.

(B, D, and F) Validation of relative localization between Calcifer and three BB markers, Centrin1 (B), SAS4 (D), and GCP3 (F), by swapping fluorescent secondary antibodies (using anti-mouse-488 and anti-rabbit-555). Scale bars, 5 μm.

(G) Proposed model of the Calcifer role in the BB integrity during axoneme exflagellation in *Plasmodium* male gametogenesis. Calcifer likely functions as a mechanical sheath wrapping the BB structure to resist axoneme-beating-induced mechanical stress, safeguarding the BB integrity.

See also Figure S6.

exflagellation for male gamete formation.[62,63] These observations further indicate that Calcifer's function is tailored to the unique demands for maintaining the mechanical stability of the basal body during axoneme exflagellation.

A comparable temporal recruitment pattern of proteins at mature basal bodies prior to axonemal beating has been noted. For instance, Fop1, Poc1, and Bld10 in *Tetrahymena thermophila* exhibit this pattern.[64,65] These proteins serve to stabilize

Please cite this article in press as: Guan et al., Mechanoregulation of basal body integrity during *Plasmodium* exflagellation, Current Biology (2026), https://doi.org/10.1016/j.cub.2026.03.068

basal bodies against the mechanical stress induced by ciliary beating, thereby maintaining structural stability. It is a rational strategy for the mechanical stability-regulating factors to be recruited to the basal bodies at the appropriate developmental phase so as to avoid interfering with axoneme assembly. The premature recruitment of such proteins might disrupt the biogenesis of either the basal body or the axoneme, underscoring the significance of tightly regulated spatiotemporal localization—a characteristic of Calcifer during male gametogenesis of *Plasmodium*.

The *in vitro* vortex assay in this study is an approach to modeling mechanical vulnerability. The results from this assay demonstrate that the Calcifer-null basal bodies at the axoneme minus end are more susceptible to mechanical perturbation. However, vortex-induced shear stress *in vitro* is not directly equivalent to the forces generated by axoneme bending *in vivo*. Therefore, this assay represents a crude surrogate mechanical challenge rather than a quantitative recapitulation of physiological forces from axoneme beating.

While our study establishes the role of Calcifer in maintaining the mechanical stability of the basal body, a crucial question remains unanswered. The exact biophysical mechanism through which Calcifer enhances mechanical stability remains unclear. Our U-ExM imaging data indicate that Calcifer wraps around the basal body, enclosing the core components (Centrin1, SAS4, and GCP3) of the basal body and the microtubules at the minus end of the axoneme. This suggests that it may function as a structural "sheath" that strengthens the basal body architecture to enhance mechanical stability. However, it is not clear whether Calcifer binds directly with basal body components, oligomerizes to form a structural scaffold, or alters the microtubule properties. Nevertheless, whether Calcifer directly interacts with these components, and if it does, the characteristics of these interactions necessitate further exploration.

In conclusion, our study reveals a mechanism through which *Plasmodium* maintains the mechanical stability of the basal body during axoneme exflagellation, which is centered on the unique basal body protein Calcifer. This work expands the functional repertoire of basal body proteins to include the regulation of mechanical stability and provides new insights into the evolutionary adaptation of eukaryotic cells to extreme mechanical challenges in critical biological processes.

RESOURCE AVAILABILITY

Lead contact

Requests for further information and resources should be directed to and will be fulfilled by the lead contact, Jing Yuan (yuanjing@xmu.edu.cn).

Materials availability

All unique/stable reagents generated in this study are available from the lead contact with a completed materials transfer agreement.

Data and code availability

- All data reported in this paper will be shared by the lead contact upon request.
- This paper does not report any original code.
- Any additional information required to reanalyze the data reported in this paper is available from the lead contact upon request.

ACKNOWLEDGMENTS

This work was supported by the National Key Research and Development Program of China (2024YFC2309700), the National Natural Science Foundation of China (32270503 to H.C. and 32170427 to J.Y.), and the 111 Project sponsored by the State Bureau of Foreign Experts and the Ministry of Education of China (BP0618017 to J.Y.).

AUTHOR CONTRIBUTIONS

J.G., H.C., and J.Y. conceived and designed the study. J.G., Y.G., and W.L. generated the genetically modified parasites. J.G. and W.L. performed phenotype analysis, protein analysis, and electron microscopy. J.G. and Y.G. conducted IFA, U-ExM, and the *in vitro* vortex assay. H.C. and J.Y. supervised the work. J.G., Y.G., and J.Y. wrote the manuscript.

DECLARATION OF INTERESTS

The authors declare no competing interests.

STAR★METHODS

Detailed methods are provided in the online version of this paper and include the following:

- KEY RESOURCES TABLE
- EXPERIMENTAL MODEL AND STUDY PARTICIPANT DETAILS
- METHOD DETAILS
  - Plasmid construction
  - Parasite transfection and genotyping
  - Negative selection with 5-fluorocytosine
  - Gametocyte induction in mice
  - Male gametocyte exflagellation assay
  - Gametocyte purification
  - Live cell imaging
  - *In vitro* ookinete culture
  - Mosquito transmission of parasites
  - Parasite genetic cross
  - Antibodies and antiserum
  - Immunofluorescence assay
  - Ultrastructure expansion microscopy (U-ExM)
  - Scanning electron microscopy
  - Transmission electron microscopy
  - Protein extraction and immunoblot
  - *In vitro* vortex assay of axoneme
  - Sequence alignment
- QUANTIFICATION AND STATISTICAL ANALYSIS

SUPPLEMENTAL INFORMATION

Supplemental information can be found online at https://doi.org/10.1016/j.cub.2026.03.068.

Received: February 4, 2026
Revised: March 24, 2026
Accepted: March 26, 2026

REFERENCES

1. WHO. (2025). World Malaria Report 2025 (WHO). https://www.who.int/publications/i/item/9789240117822
2. Taylor, L.H., and Read, A.F. (1997). Why so few transmission stages? Reproductive restraint by malaria parasites. Parasitol. Today *13*, 135–140. https://doi.org/10.1016/s0169-4758(97)89810-9.

3. Guttery, D.S., Roques, M., Holder, A.A., and Tewari, R. (2015). Commit and transmit: molecular players in *Plasmodium* sexual development and zygote differentiation. Trends Parasitol. *31*, 676–685. https://doi.org/10.1016/j.pt.2015.08.002.

4. Sinden, R.E. (1983). The cell biology of sexual development in *Plasmodium*. Parasitology *86*, 7–28. https://doi.org/10.1017/s0031182000050824.

5. Bennink, S., Kiesow, M.J., and Pradel, G. (2016). The development of malaria parasites in the mosquito midgut. Cell. Microbiol. *18*, 905–918. https://doi.org/10.1111/cmi.12604.

6. Janse, C.J., Van der Klooster, P.F., Van der Kaay, H.J., Van der Ploeg, M., and Overdulve, J.P. (1986). Rapid repeated DNA replication during microgametogenesis and DNA synthesis in young zygotes of *Plasmodium berghei*. Trans. R. Soc. Trop. Med. Hyg. *80*, 154–157. https://doi.org/10.1016/0035-9203(86)90219-1.

7. Sinden, R.E. (1991). Mitosis and meiosis in malarial parasites. Acta Leiden. *60*, 19–27.

8. Francia, M.E., Dubremetz, J.-F., and Morrissette, N.S. (2015). Basal body structure and composition in the apicomplexans *Toxoplasma* and *Plasmodium*. Cilia *5*, 3. https://doi.org/10.1186/s13630-016-0025-5.

9. Sinden, R.E., Talman, A., Marques, S.R., Wass, M.N., and Sternberg, M.J. (2010). The flagellum in malarial parasites. Curr. Opin. Microbiol. *13*, 491–500. https://doi.org/10.1016/j.mib.2010.05.016.

10. Rashpa, R., and Brochet, M. (2022). Expansion microscopy of *Plasmodium* gametocytes reveals the molecular architecture of a bipartite microtubule organisation centre coordinating mitosis with axoneme assembly. PLOS Pathog. *18*, e1010223. https://doi.org/10.1371/journal.ppat.1010223.

11. Zeeshan, M., Rashpa, R., Ferguson, D.J., Mckeown, G., Nugmanova, R., Subudhi, A.K., Beyeler, R., Pashley, S.L., Markus, R., Brady, D., et al. (2024). *Plasmodium* NEK1 coordinates MTOC organisation and kinetochore attachment during rapid mitosis in male gamete formation. PLOS Biol. *22*, e3002802. https://doi.org/10.1371/journal.pbio.3002802.

12. Zeeshan, M., Blatov, I., Yanase, R., Ferguson, D.J.P., Pashley, S.L., Chahine, Z., Yamaryo-Botté, Y., Mishra, A., Marche, B., Bhanvadia, S., et al. (2025). A novel SUN1-ALLAN complex coordinates segregation of the bipartite MTOC across the nuclear envelope during rapid closed mitosis in *Plasmodium berghei*. eLife *14*, RP106537. https://doi.org/10.7554/eLife.106537.

13. Sinden, R.E., Canning, E.U., Bray, R.S., and Smalley, M.E. (1978). Gametocyte and gamete development in *Plasmodium falciparum*. Proc. R. Soc. Lond. B Biol. Sci. *201*, 375–399. https://doi.org/10.1098/rspb.1978.0051.

14. Zeeshan, M., Ferguson, D.J., Abel, S., Burrrell, A., Rea, E., Brady, D., Daniel, E., Delves, M., Vaughan, S., Holder, A.A., et al. (2019). Kinesin-8B controls basal body function and flagellum formation and is key to malaria transmission. Life Sci. Alliance *2*, e201900488. https://doi.org/10.26508/lsa.201900488.

15. Zeeshan, M., Shilliday, F., Liu, T., Abel, S., Mourier, T., Ferguson, D.J.P., Rea, E., Stanway, R.R., Roques, M., Williams, D., et al. (2019). *Plasmodium* kinesin-8X associates with mitotic spindles and is essential for oocyst development during parasite proliferation and transmission. PLOS Pathog. *15*, e1008048. https://doi.org/10.1371/journal.ppat.1008048.

16. Hair, M., Moreira-Leite, F., Ferguson, D.J.P., Zeeshan, M., Tewari, R., and Vaughan, S. (2023). Atypical flagella assembly and haploid genome coiling during male gamete formation in *Plasmodium*. Nat. Commun. *14*, 8263. https://doi.org/10.1038/s41467-023-43877-w.

17. Gerald, N., Mahajan, B., and Kumar, S. (2011). Mitosis in the human malaria parasite *Plasmodium falciparum*. Eukaryot. Cell *10*, 474–482. https://doi.org/10.1128/ec.00314-10.

18. Yang, S., Cai, M., Huang, J., Zhang, S., Mo, X., Jiang, K., Cui, H., and Yuan, J. (2023). EB1 decoration of microtubule lattice facilitates spindle-kinetochore lateral attachment in *Plasmodium* male gametogenesis. Nat. Commun. *14*, 2864. https://doi.org/10.1038/s41467-023-38516-3.

19. Sinden, R.E., and Croll, N.A. (1975). Cytology and kinetics of microgametogenesis and fertilization in *Plasmodium yoelii* nigeriensis. Parasitology *70*, 53–65. https://doi.org/10.1017/s0031182000048861.

20. Dash, M., Sachdeva, S., Bansal, A., and Sinha, A. (2022). Gametogenesis in *Plasmodium*: delving deeper to connect the dots. Front. Cell. Infect. Microbiol. *12*, 877907. https://doi.org/10.3389/fcimb.2022.877907.

21. Talman, A.M., Prieto, J.H., Marques, S., Ubaida-Mohien, C., Lawniczak, M., Wass, M.N., Xu, T., Frank, R., Ecker, A., Stanway, R.S., et al. (2014). Proteomic analysis of the *Plasmodium* male gamete reveals the key role for glycolysis in flagellar motility. Malar. J. *13*, 315. https://doi.org/10.1186/1475-2875-13-315.

22. Sorokin, S.P. (1968). Reconstructions of centriole formation and ciliogenesis in mammalian lungs. J. Cell Sci. *3*, 207–230. https://doi.org/10.1242/jcs.3.2.207.

23. Carvalho-Santos, Z., Azimzadeh, J., Pereira-Leal, J.B., and Bettencourt-Dias, M. (2011). Evolution: Tracing the origins of centrioles, cilia, and flagella. J. Cell Biol. *194*, 165–175. https://doi.org/10.1083/jcb.201011152.

24. Wu, C.T., Chen, H.Y., and Tang, T.K. (2018). Myosin-Va is required for preciliary vesicle transportation to the mother centriole during ciliogenesis. Nat. Cell Biol. *20*, 175–185. https://doi.org/10.1038/s41556-017-0018-7.

25. Breslow, D.K., and Holland, A.J. (2019). Mechanism and regulation of centriole and cilium biogenesis. Annu. Rev. Biochem. *88*, 691–724. https://doi.org/10.1146/annurev-biochem-013118-111153.

26. Sinden, R.E. (2015). The cell biology of malaria infection of mosquito: advances and opportunities. Cell. Microbiol. *17*, 451–466. https://doi.org/10.1111/cmi.12413.

27. Hodges, M.E., Scheumann, N., Wickstead, B., Langdale, J.A., and Gull, K. (2010). Reconstructing the evolutionary history of the centriole from protein components. J. Cell Sci. *123*, 1407–1413. https://doi.org/10.1242/jcs.064873.

28. Ramakrishnan, C., Fort, C., Marques, S.R., Ferguson, D.J.P., Gransagne, M., Baum, J., Chaouch, S., Mouray, E., Kohl, L., Wheeler, R.J., et al. (2023). Radial spoke protein 9 is necessary for axoneme assembly in *Plasmodium* but not in trypanosomatid parasites. J. Cell Sci. *136*, jcs260655. https://doi.org/10.1242/jcs.260655.

29. Sinden, R.E., Canning, E.U., and Spain, B. (1976). Gametogenesis and fertilization in *Plasmodium yoelii* nigeriensis: a transmission electron microscope study. Proc. R. Soc. Lond. B Biol. Sci. *193*, 55–76. https://doi.org/10.1098/rspb.1976.0031.

30. Yang, S., Ma, S., Yuan, C., Li, Z., Ji, F., Yao, L., Cui, H., Guo, Q., and Yuan, J. (2025). A basal body microtubule singlet-to-doublet transition in *Plasmodium* male gametogenesis. Nat. Commun. *16*, 9150. https://doi.org/10.1038/s41467-025-64158-8.

31. Tomasina, R., González, F.C., and Francia, M.E. (2021). Structural and functional insights into the microtubule organizing centers of *Toxoplasma gondii* and *Plasmodium* spp. Microorganisms *9*, 2503. https://doi.org/10.3390/microorganisms9122503.

32. Greenan, G.A., Vale, R.D., and Agard, D.A. (2020). Electron cryotomography of intact motile cilia defines the basal body to axoneme transition. J. Cell Biol. *219*, e201907060. https://doi.org/10.1083/jcb.201907060.

33. Garreau de Loubresse, N., Ruiz, F., Beisson, J., and Klotz, C. (2001). Role of delta-tubulin and the C-tubule in assembly of *Paramecium* basal bodies. BMC Cell Biol. *2*, 4. https://doi.org/10.1186/1471-2121-2-4.

34. Li, S., Fernandez, J.J., Marshall, W.F., and Agard, D.A. (2012). Three-dimensional structure of basal body triplet revealed by electron cryo-tomography. EMBO J. *31*, 552–562. https://doi.org/10.1038/emboj.2011.460.

35. Lasonder, E., Rijpma, S.R., van Schaijk, B.C.L., Hoeijmakers, W.A.M., Kensche, P.R., Gresnigt, M.S., Italiaander, A., Vos, M.W., Woestenenk, R., Bousema, T., et al. (2016). Integrated transcriptomic and proteomic analyses of *P. falciparum* gametocytes: molecular insight into sex-specific processes and translational repression. Nucleic Acids Res. *44*, 6087–6101. https://doi.org/10.1093/nar/gkw536.

36. Yeoh, L.M., Goodman, C.D., Mollard, V., McFadden, G.I., and Ralph, S.A. (2017). Comparative transcriptomics of female and male gametocytes in *Plasmodium berghei* and the evolution of sex in alveolates. BMC Genomics *18*, 734. https://doi.org/10.1186/s12864-017-4100-0.

37. Guan, J., Wu, P., Mo, X., Zhang, X., Liang, W., Zhang, X., Jiang, L., Li, J., Cui, H., and Yuan, J. (2024). An axonemal intron splicing program sustains *Plasmodium* male development. Nat. Commun. *15*, 4697. https://doi.org/10.1038/s41467-024-49002-9.

38. Russell, A.J.C., Sanderson, T., Bushell, E., Talman, A.M., Anar, B., Girling, G., Hunziker, M., Kent, R.S., Martin, J.S., Metcalf, T., et al. (2023). Regulators of male and female sexual development are critical for the transmission of a malaria parasite. Cell Host Microbe *31*, 305–319. https://doi.org/10.1016/j.chom.2022.12.011.

39. Rawlings, D.J., Fujioka, H., Fried, M., Keister, D.B., Aikawa, M., and Kaslow, D.C. (1992). Alpha-tubulin II is a male-specific protein in *Plasmodium falciparum*. Mol. Biochem. Parasitol. *56*, 239–250. https://doi.org/10.1016/0166-6851(92)90173-h.

40. Tewari, R., Dorin, D., Moon, R., Doerig, C., and Billker, O. (2005). An atypical mitogen-activated protein kinase controls cytokinesis and flagellar motility during male gamete formation in a malaria parasite. Mol. Microbiol. *58*, 1253–1263. https://doi.org/10.1111/j.1365-2958.2005.04793.x.

41. Reininger, L., Billker, O., Tewari, R., Mukhopadhyay, A., Fennell, C., Dorin-Semblat, D., Doerig, C., Goldring, D., Harmse, L., Ranford-Cartwright, L., et al. (2005). A NIMA-related protein kinase is essential for completion of the sexual cycle of malaria parasites. J. Biol. Chem. *280*, 31957–31964. https://doi.org/10.1074/jbc.M504523200.

42. Mahajan, B., Selvapandiyan, A., Gerald, N.J., Majam, V., Zheng, H., Wickramarachchi, T., Tiwari, J., Fujioka, H., Moch, J.K., Kumar, N., et al. (2008). Centrins, cell cycle regulation proteins in human malaria parasite *Plasmodium falciparum*. J. Biol. Chem. *283*, 31871–31883. https://doi.org/10.1074/jbc.M800028200.

43. Zeeshan, M., Brady, D., Markus, R., Vaughan, S., Ferguson, D., Holder, A.A., and Tewari, R. (2022). *Plasmodium* SAS4: basal body component of male cell which is dispensable for parasite transmission. Life Sci. Alliance *5*, e202101329. https://doi.org/10.26508/lsa.202101329.

44. Bertiaux, E., Balestra, A.C., Bournonville, L., Louvel, V., Maco, B., Soldati-Favre, D., Brochet, M., Guichard, P., and Hamel, V. (2021). Expansion microscopy provides new insights into the cytoskeleton of malaria parasites including the conservation of a conoid. PLOS Biol. *19*, e3001020. https://doi.org/10.1371/journal.pbio.3001020.

45. Haase, R., Puthenpurackal, A., Maco, B., Guérin, A., and Soldati-Favre, D. (2024). γ-tubulin complex controls the nucleation of tubulin-based structures in Apicomplexa. Mol. Biol. Cell *35*, ar121. https://doi.org/10.1091/mbc.E24-03-0100.

46. Kubo, T., Yanagisawa, H.A., Yagi, T., Hirono, M., and Kamiya, R. (2010). Tubulin polyglutamylation regulates axonemal motility by modulating activities of inner-arm dyneins. Curr. Biol. *20*, 441–445. https://doi.org/10.1016/j.cub.2009.12.058.

47. Liu, C., Li, Z., Jiang, Y., Cui, H., and Yuan, J. (2018). Generation of *Plasmodium yoelii* malaria parasite carrying double fluorescence reporters in gametocytes. Mol. Biochem. Parasitol. *224*, 37–43. https://doi.org/10.1016/j.molbiopara.2018.07.010.

48. King, S.M. (2016). Axonemal dynein arms. Cold Spring Harb. Perspect. Biol. *8*, a028100. https://doi.org/10.1101/cshperspect.a028100.

49. Gopalakrishnan, J., Mennella, V., Blachon, S., Zhai, B., Smith, A.H., Megraw, T.L., Nicastro, D., Gygi, S.P., Agard, D.A., and Avidor-Reiss, T. (2011). Sas-4 provides a scaffold for cytoplasmic complexes and tethers them in a centrosome. Nat. Commun. *2*, 359. https://doi.org/10.1038/ncomms1367.

50. Guichard, P., Chrétien, D., Marco, S., and Tassin, A.M. (2010). Procentriole assembly revealed by cryo-electron tomography. EMBO J. *29*, 1565–1572. https://doi.org/10.1038/emboj.2010.45.

51. Winey, M., and O'Toole, E. (2014). Centriole structure. Philos. Trans. R. Soc. Lond., B Biol. Sci. *369*, 20130457. https://doi.org/10.1098/rstb.2013.0457.

52. Tanos, B.E., Yang, H.J., Soni, R., Wang, W.J., Macaluso, F.P., Asara, J.M., and Tsou, M.F.B. (2013). Centriole distal appendages promote membrane docking, leading to cilia initiation. Genes Dev. *27*, 163–168. https://doi.org/10.1101/gad.207043.112.

53. Mansour, F., Boivin, F.J., Shaheed, I.B., Schueler, M., and Schmidt-Ott, K.M. (2021). The role of centrosome distal appendage proteins (DAPs) in nephronophthisis and ciliogenesis. Int. J. Mol. Sci. *22*, 12253. https://doi.org/10.3390/ijms222212253.

54. Tateishi, K., Nishida, T., Inoue, K., and Tsukita, S. (2017). Three-dimensional organization of layered apical cytoskeletal networks associated with mouse airway tissue development. Sci. Rep. *7*, 43783. https://doi.org/10.1038/srep43783.

55. Pan, J., You, Y., Huang, T., and Brody, S.L. (2007). RhoA-mediated apical actin enrichment is required for ciliogenesis and promoted by Foxj1. J. Cell Sci. *120*, 1868–1876. https://doi.org/10.1242/jcs.005306.

56. Yang, T.T., Chong, W.M., Wang, W.J., Mazo, G., Tanos, B., Chen, Z., Tran, T.M.N., Chen, Y.D., Weng, R.R., Huang, C.E., et al. (2018). Super-resolution architecture of mammalian centriole distal appendages reveals distinct blade and matrix functional components. Nat. Commun. *9*, 2023. https://doi.org/10.1038/s41467-018-04469-1.

57. Höög, J.L., Lacomble, S., O'Toole, E.T., Hoenger, A., McIntosh, J.R., and Gull, K. (2014). Modes of flagellar assembly in *Chlamydomonas reinhardtii* and *Trypanosoma brucei*. eLife *3*, e01479. https://doi.org/10.7554/eLife.01479.

58. Bastin, P., MacRae, T.H., Francis, S.B., Matthews, K.R., and Gull, K. (1999). Flagellar morphogenesis: protein targeting and assembly in the paraflagellar rod of trypanosomes. Mol. Cell. Biol. *19*, 8191–8200. https://doi.org/10.1128/mcb.19.12.8191.

59. Weber, K., Waletzky, A., Fendl, D., Ordóñez, P., Takawale, P., Hein, F., Riedel, W., König, A., Kunze, M., Leoni, A.L., et al. (2014). New method for sperm evaluation by 3-dimensional laser scanning microscopy in different laboratory animal species. Int. J. Toxicol. *33*, 353–361. https://doi.org/10.1177/1091581814545243.

60. Galen, S.C., Borner, J., Martinsen, E.S., Schaer, J., Austin, C.C., West, C.J., and Perkins, S.L. (2018). The polyphyly of *Plasmodium*: comprehensive phylogenetic analyses of the malaria parasites (order Haemosporida) reveal widespread taxonomic conflict. R. Soc. Open Sci. *5*, 171780. https://doi.org/10.1098/rsos.171780.

61. Martinsen, E.S., Perkins, S.L., and Schall, J.J. (2008). A three-genome phylogeny of malaria parasites (*Plasmodium* and closely related genera): evolution of life-history traits and host switches. Mol. Phylogenet. Evol. *47*, 261–273. https://doi.org/10.1016/j.ympev.2007.11.012.

62. Ejotre, I., Reeder, D.M., Matuschewski, K., and Schaer, J. (2021). Hepatocystis. Trends Parasitol. *37*, 456–457. https://doi.org/10.1016/j.pt.2020.07.015.

63. Valkiūnas, G., and Iezhova, T.A. (2022). Keys to the avian *Haemoproteus* parasites (Haemosporida, Haemoproteidae). Malar. J. *21*, 269. https://doi.org/10.1186/s12936-022-04235-1.

64. Bayless, B.A., Giddings, T.H., Jr., Winey, M., and Pearson, C.G. (2012). Bld10/Cep135 stabilizes basal bodies to resist cilia-generated forces. Mol. Biol. Cell *23*, 4820–4832. https://doi.org/10.1091/mbc.E12-08-0577.

65. Bayless, B.A., Galati, D.F., Junker, A.D., Backer, C.B., Gaertig, J., and Pearson, C.G. (2016). Asymmetrically localized proteins stabilize basal bodies against ciliary beating forces. J. Cell Biol. *215*, 457–466. https://doi.org/10.1083/jcb.201604135.

66. Gao, H., Yang, Z., Wang, X., Qian, P., Hong, R., Chen, X., Su, X.-Z., Cui, H., and Yuan, J. (2018). ISP1-anchored polarization of GCβ/CDC50A complex initiates malaria ookinete gliding motility. Curr. Biol. *28*, 2763–2776. https://doi.org/10.1016/j.cub.2018.06.069.

67. Zhang, C., Xiao, B., Jiang, Y., Zhao, Y., Li, Z., Gao, H., Ling, Y., Wei, J., Li, S., Lu, M., et al. (2014). Efficient editing of malaria parasite genome using

the CRISPR/Cas9 system. mBio *5*, e01414-14. https://doi.org/10.1128/mBio.01414-14.

68. Zhang, C., Gao, H., Yang, Z., Jiang, Y., Li, Z., Wang, X., Xiao, B., Su, X.-Z., Cui, H., and Yuan, J. (2017). CRISPR/Cas9 mediated sequential editing of genes critical for ookinete motility in *Plasmodium yoelii*. Mol. Biochem. Parasitol. *212*, 1–8. https://doi.org/10.1016/j.molbiopara.2016.12.010.

69. Jiang, Y., Wei, J., Cui, H., Liu, C., Zhi, Y., Jiang, Z., Li, Z., Li, S., Yang, Z., Wang, X., et al. (2020). An intracellular membrane protein GEP1 regulates xanthurenic acid induced gametogenesis of malaria parasites. Nat. Commun. *11*, 1764. https://doi.org/10.1038/s41467-020-15479-3.

70. Gambarotto, D., Hamel, V., and Guichard, P. (2021). Ultrastructure expansion microscopy (U-ExM). Methods Cell Biol. *161*, 57–81. https://doi.org/10.1016/bs.mcb.2020.05.006.

Please cite this article in press as: Guan et al., Mechanoregulation of basal body integrity during *Plasmodium* exflagellation, Current Biology (2026), https://doi.org/10.1016/j.cub.2026.03.068

STAR★METHODS

KEY RESOURCES TABLE

REAGENT or RESOURCE	SOURCE	IDENTIFIER
Antibodies		
Rabbit anti-HA	Cell Signaling Technology	Cat#3724S; RRID: AB_1549585
Rabbit anti-mCherry	Abcam	Cat#ab167453; RRID: AB_2571870
Rabbit anti-Myc	Cell Signaling Technology	Cat#2272S; RRID: AB_10692100
Rabbit anti-Polyglutamate chain (PolyE)	AdipoGen	Cat#AG-25B-0030; RRID: AB_2490540
Mouse anti-HA	Santa Cruz Biotechnology	Cat#sc-57592; RRID: AB_629568
Mouse anti-Myc	Cell Signaling Technology	Cat#2276S; RRID: AB_331783
Mouse anti-αII-Tubulin	Sigma-Aldrich	Cat#T6199; RRID: AB_477583
Alexa Fluor 555 goat anti-rabbit IgG	Thermo Fisher Scientific	Cat#A-21428; RRID: AB_2535849
Alexa Fluor 488 goat anti-rabbit IgG	Thermo Fisher Scientific	Cat#A-31566; RRID: AB_10374301
Alexa Fluor 555 goat anti-mouse IgG	Thermo Fisher Scientific	Cat#A-21422; RRID: AB_2535844
Alexa Fluor 488 goat anti-mouse IgG	Thermo Fisher Scientific	Cat#A-11001; RRID: AB_2534069
HRP-conjugated goat anti-rabbit IgG	Abcam	Cat#ab6721; RRID: AB_955447
HRP-conjugated goat anti-mouse IgG	Abcam	Cat#ab6789; RRID: AB_955439
Rabbit anti-BiP serum	Gao et al.[66]	N/A
Rabbit anti-P28 serum	Gao et al.[66]	N/A
Chemicals, peptides, and recombinant proteins		
Nycodenz	Axis-shield	Cat#66108-95-0
5-fluorocytosine	Sigma-Aldrich	Cat#F6627
Phenylhydrazine	Sangon Biotech	Cat#A600705-0025
Giemsa solution	Sigma-Aldrich	Cat#GS80
Xanthurenic acid	Sigma-Aldrich	Cat#D120804
Sulfadiazine	Sigma-Aldrich	Cat#S8626
Hoechst 33342	Thermo Fisher Scientific	Cat#62249
RPMI 1640 medium liquid	Hyclone	Cat#SH30809.01B
NHS-ester dye	Thermo Fisher Scientific	Cat#A30000
Protease inhibitor cocktail	MedChemExpress	Cat#HY-K0010
Enhanced chemiluminescence	LABLEAD	Cat#E1060
Experimental models: Organisms/strains		
P.yoelii 17XNL strain	Zhang et al.[67]	N/A
P.yoelii 17XNL/*DFsc7* strain	Liu et al.[45]	N/A
Other modified parasite lines listed in Table S1	This paper	N/A

(*Continued on next page*)

Please cite this article in press as: Guan et al., Mechanoregulation of basal body integrity during *Plasmodium* exflagellation, Current Biology (2026), https://doi.org/10.1016/j.cub.2026.03.068

Continued

REAGENT or RESOURCE	SOURCE	IDENTIFIER
Oligonucleotides		
Oligonucleotides and primers listed in Table S2	This paper	N/A
Recombinant DNA		
pYCm Cas9 plasmid	Zhang et al.[68]	N/A
Software and algorithms		
Graphpad Prism 8.0.2	GraphPad Software	https://www.graphpad.com/
Imaris 10.2.0	Oxford Instruments	https://imaris.oxinst.com/
MEGA11	MEGA Software	https://www.megasoftware.net/
BioEdit 7.2.5	Tom Hall	N/A

EXPERIMENTAL MODEL AND STUDY PARTICIPANT DETAILS

Animal experiments in this study were approved by the Committee for Care and Use of Laboratory Animals of Xiamen University (XMULAC20230333). Female ICR mice (5-6 weeks old) were obtained from the Animal Care Center of Xiamen University and housed in a controlled environment (22-24°C, 45-65% humidity, 12-hour light/dark cycle). These mice were used for parasite propagation, drug selection, cloning, and mosquito feeding. *Anopheles stephensi* (Hor strain) mosquito larvae were reared under controlled conditions (28°C, 80% humidity, 12-hour light/dark cycle). Adult mosquitoes were maintained on a 10% (w/v) sucrose solution containing 0.05% 4-aminobenzoic acid at 23°C.

METHOD DETAILS

Plasmid construction

CRISPR/Cas9-mediated genome editing was performed using the pYCm plasmid.[68] For gene tagging, 5′ and 3′ homologous sequences (400-700 bp) flanking the target gene's insertion site were PCR-amplified and cloned into pYCm. Epitope tags (HA, 6HA, 4Myc, or mCherry) were inserted in-frame between the homologous arms. For gene deletion or truncation, sequences flanking the target region were amplified to serve as left and right homologous arms. At least three small guide RNAs (sgRNAs) were designed for each construct. Paired sgRNA oligonucleotides were denatured at 95°C for 3 min, annealed at room temperature for 5 min, and ligated into pYCm. All the genetically modified parasite lines generated are listed in Table S1. All primers and oligonucleotides used are listed in Table S2.

Parasite transfection and genotyping

Parasite transfection and genotyping were performed as previously described.[68,67] Briefly, schizonts were purified from infected mice using a 60% Nycodenz gradient and electroporated with 5 μg plasmid using a Nucleofector 2b Device (Lonza, Germany). Transfected schizonts were immediately injected intravenously into a naïve mouse. Pyrimethamine (6 mg/L in drinking water) was administered 24 h post-transfection for selection. Drug-resistant parasites typically appeared within 7 days. Blood was collected from the tail vein of infected mice and lysed with 1% saponin in PBS. Parasites were pelleted by centrifugation at 13,000 *g* for 1 minute, washed twice with PBS, and boiled at 95°C for 10 minutes. After centrifugation, the supernatant containing genomic DNA was used for PCR-based genotyping. For each gene modification, diagnostic PCR targeting both 5′ and 3′ recombination sites was conducted to confirm successful integration. Parasite cloned lines were obtained by limiting dilution. All primers are listed in Table S2. Genotyping PCR confirmation results are provided in Figure S7.

Negative selection with 5-fluorocytosine

To eliminate pYCm plasmids in preparation for the subsequent gene editing, negative selection with 5-fluorocytosine was applied.[68] Mice infected with the parasite clones were provided with drinking water containing 2 mg/ml of 5-fluorocytosine (Sigma-Aldrich, cat#F6627). After approximately five days, the removal of the pYCm plasmids in surviving parasites was confirmed via PCR. The parasite cloned lines were generated via limiting dilution. Pyrimethamine treatment was further applied to confirm plasmid clearance.

Gametocyte induction in mice

ICR mice were intraperitoneally injected with phenylhydrazine (80 μg/g body weight, Sangon Biotech, cat#A600705-0025) to induce reticulocytosis. Three days post-treatment, mice were infected with 5×10^6 asexual blood stage parasites via tail vein injection. Male

Please cite this article in press as: Guan et al., Mechanoregulation of basal body integrity during *Plasmodium* exflagellation, Current Biology (2026), https://doi.org/10.1016/j.cub.2026.03.068

and female gametocytes were quantified on Giemsa-stained thin blood films. Peak gametocytemia usually appears on day 3 post-infection and was calculated as the proportion of male or female gametocytes among total parasitized erythrocytes.

Male gametocyte exflagellation assay

2.5 μl of mouse tail blood with gametocytes was mixed with 100 μl of exflagellation medium, consisting of RPMI 1640 supplemented with 100 μM xanthurenic acid (XA, Sigma, cat#D120804), 2 U/ml heparin, and pH 7.4. The mixture was incubated at 22°C for 10 minutes. The numbers of exflagellation centers (ECs) and total red blood cells were counted in a 1×1 mm area of a hemocytometer under a light microscope. The exflagellation rate was calculated as the number of ECs per 100 male gametocytes.

Gametocyte purification

Gametocyte purification was performed as previously described.[69] ICR mice pretreated with phenylhydrazine were infected with 5×10^6 asexual blood stage parasites. Starting from 2 days post-infection, mice were orally administered sulfadiazine (0.12 mg/day; Sigma, cat#S8626) for 2 days to eliminate asexual blood stage parasites. On day 3 post-infection, approximately 1 ml of blood was collected from the orbital sinus and suspended in 6 ml of gametocyte maintenance buffer (GMB), consisting of 137 mM NaCl, 4 mM KCl, 1 mM $CaCl_2$, 20 mM glucose, 20 mM HEPES, 4 mM $NaHCO_3$, and 0.1% BSA (pH 7.2). The 7 ml sample was layered onto a 2 ml cushion of 48% Nycodenz in GMB in a 15 ml centrifuge tube. The Nycodenz solution contained 27.6% w/v Nycodenz in 5 mM Tris-HCl (pH 7.2), 3 mM KCl, and 0.3 mM EDTA. After centrifugation at 1900 *g* for 20 minutes, gametocytes were collected from the interface layer and washed twice with GMB for further use.

Live cell imaging

Live parasite cells of the asexual blood parasites, gametocytes, and ookinetes were resuspended in PBS and stained with 2 μM Hoechst 33342 (Thermo Fisher Scientific, cat#62249) for 10 min. Images were captured using a Zeiss LSM 980 confocal microscope. For time-lapse imaging of male gamete formation, purified gametocytes were suspended in 200 μl of exflagellation medium and transferred to a 15 mm glass-bottom dish. Images were captured at 22°C using a Leica Stellaris 8 STED microscope. To record the male gamete release process in the same focal plane, low-melting-point agarose (1% working concentration, BBI Life Science, cat#9012-36-6) was added to the exflagellation medium to minimize gametocyte movement. The agarose was dissolved at 95°C and cooled below 37°C before being mixed with gametocytes. The mixture was spread onto a glass-bottom dish and imaged under identical conditions.

In vitro ookinete culture

Approximately 1 ml mouse blood samples containing gametocytes were collected and immediately mixed with 10 ml of ookinete culture medium. The medium consisted of RPMI 1640 supplemented with 25 mM HEPES, 10% fetal calf serum, 100 μM XA, pH 8.0. Cultures were incubated at 22°C for 16-20 hours and analyzed by Giemsa-stained thin blood smears. Ookinete conversion rate was calculated as the number of ookinetes per 100 female gametocytes.

Mosquito transmission of parasites

Approximately 100 female mosquitoes in one cage were blood-fed for 30 minutes on an anesthetized mouse with 4-6% gametocytaemia. At day 7 post blood feeding, the mosquito midguts were dissected and stained with 0.1% mercurochrome for oocyst observation. At day 14 post blood feeding, the mosquito salivary glands were dissected. Sporozoites from thirty mosquito salivary glands were collected and counted using a hemocytometer, and the average number of sporozoites per mosquito was calculated.

Parasite genetic cross

Δ*map2* is a male gamete-deficient line while Δ*nek4* is a female gamete-deficient line. A parasite mixture containing an equal amount (3×10^6) of asexual blood stage parasites from two different parasite lines was prepared for mouse infection. Three days after phenylhydrazine treatment, mice were intravenously injected with the parasite mixture. Three days after infection, blood containing gametocytes was collected for *in vitro* gametocyte-to-ookinete development.

Antibodies and antiserum

The following primary antibodies were used: rabbit anti-HA (Cell Signaling Technology, cat#3724S; IFA 1:1000; IB 1:1000; U-ExM 1:500), rabbit anti-mCherry (Abcam, cat# ab167453; IFA 1:1000; U-ExM 1:500), rabbit anti-Myc (Cell Signaling Technology, cat#2272S; IFA 1:1000; U-ExM 1:500), rabbit anti-Polyglutamate chain (PolyE) (AdipoGen, cat#AG-25B-0030, IFA 1:1000; U-ExM 1:500), mouse anti-HA (Santa Cruz Biotechnology, cat#sc-57592; IFA 1:200), mouse anti-Myc (Cell Signaling Technology, cat#2276S; IFA 1:1000; IB 1:1000; U-ExM 1:500) and mouse anti-αII-Tubulin (Sigma-Aldrich, cat#T6199; IFA 1:1000; U-ExM 1:500). Secondary antibodies included: Alexa Fluor 555 goat anti-rabbit IgG (Thermo Fisher Scientific, cat#A-21428; IFA 1:1000; U-ExM 1:500), Alexa Fluor 488 goat anti-rabbit IgG (Thermo Fisher Scientific, cat#A-31566; IFA 1:1000; U-ExM 1:500), Alexa Fluor 555 goat anti-mouse IgG (Thermo Fisher Scientific, cat# A-21422; IFA 1:1000; U-ExM 1:500), Alexa Fluor 488 goat anti-mouse IgG (Thermo Fisher Scientific, cat#A-11001; IFA 1:1000; U-ExM 1:500), HRP-conjugated goat anti-rabbit IgG (Abcam, cat#ab6721; IB 1:5000) and HRP-conjugated goat anti-mouse IgG (Abcam, cat#ab6789; IB 1:5000). In-house antiserum included rabbit anti-BiP (IB 1:1000) and rabbit anti-P28 (IFA 1:1000).[66]

Please cite this article in press as: Guan et al., Mechanoregulation of basal body integrity during *Plasmodium* exflagellation, Current Biology (2026), https://doi.org/10.1016/j.cub.2026.03.068

Immunofluorescence assay

Parasites were fixed in 4% paraformaldehyde in PBS and seeded onto poly-L-lysine-coated coverslips by centrifugation (550 *g*, 5 minutes). Cells were permeabilized with 0.1% Triton X-100 in PBS for 10 minutes and blocked with 5% BSA/PBS at room temperature for 1 hour. Primary antibodies diluted in 5% BSA/PBS were added for 1 hour, followed by three PBS washes and incubation with fluorescently labeled secondary antibodies for another hour. Hoechst 33342 (1:5000 in PBS) was used to stain DNA for 15 minutes. Coverslips were mounted in 90% glycerol and sealed. Images were captured using a Zeiss LSM 980 confocal microscope.

Ultrastructure expansion microscopy (U-ExM)

U-ExM was performed as previously described.[70] Gametocytes were fixed in 4% paraformaldehyde in PBS and transferred to poly-D-lysine-coated coverslips. After centrifugation, samples were incubated overnight at 37°C in 1.4% formaldehyde and 2% acrylamide in PBS. Gels were polymerized in a monomer solution (23% sodium acrylate, 10% acrylamide, 0.1% N, N'-methylenbisacrylamide in PBS with tetramethylethylenediamine and ammonium persulfate) at 37°C for 1 hour. Gels were detached in denaturation buffer (200 mM SDS, 200 mM NaCl, 50 mM Tris-HCl, pH 8.8) and incubated at 95°C for 30 minutes for denaturation. Following overnight expansion in ddH_2O, gels were rinsed in PBS, cut into quarters, and stained with primary antibodies in 2% BSA/PBS for 3 hours at room temperature. After PBS washes, secondary antibodies were applied under the same conditions. In some experiments, the parasites were stained with the NHS-ester dye (Thermo Fisher, cat#A30000, 10 μg/mL in PBS) for 3 h. Gels were re-expanded in ddH_2O and trimmed into ~5 × 5 mm blocks. Imaging was conducted using Zeiss LSM 980 and Leica Stellaris 8 STED microscope.

Scanning electron microscopy

Purified gametocytes were fixed overnight at 4°C using 2.5% glutaraldehyde in 0.1 M phosphate buffer. After three washes with PBS, samples were fixed in 1% osmium tetroxide for 2 hours at 4°C. Specimens were dehydrated through a graded acetone series, dried using a CO_2 critical point dryer (K850, Emitech, UK), and coated with gold using a sputter coater (JFC-1600, JEOL, Japan). Imaging was performed using a scanning electron microscope (SUPRA55 SAPPHIRE, ZEISS, Germany).

Transmission electron microscopy

Activated gametocytes were fixed overnight at 4 °C in 2.5% glutaraldehyde in 0.1 M phosphate buffer, and then fixed in 1% osmium tetroxide at 4 °C for 2 hours. Samples were stained *en bloc* with uranyl acetate, dehydrated through a graded ethanol series, and embedded in Spurr's resin. Ultrathin sections were cut, post-stained with uranyl acetate and lead citrate, and imaged using a transmission electron microscope (HT-7800, Hitachi, Japan).

Protein extraction and immunoblot

Parasites were lysed in buffer (0.1% SDS, 20 mM Tris-HCl pH 8.0, 50 mM NaCl, 1 mM DTT, and protease inhibitor cocktail; MedChemExpress, cat#HY-K0010) for 10 minutes. After ultrasonication, the lysates were incubated on ice for 10 minutes and then centrifuged at 14,000 *g* for 10 minutes at 4°C. Supernatants were mixed with SDS-PAGE loading buffer, boiled at 95°C for 5 minutes, separated by SDS-PAGE, and transferred to PVDF membranes (Millipore, cat#IPVH00010). Membranes were blocked overnight at 4°C in 5% milk/TBST, then incubated with primary antibodies for 1 hour at room temperature, followed by HRP-conjugated secondary antibodies. Signals were detected using enhanced chemiluminescence (LABLEAD, cat#E1060).

In vitro vortex assay of axoneme

Purified gametocytes (2×10^7) were suspended in 1 ml exflagellation medium and activated at 22°C for 5 minutes. Cells were centrifuged at 1,000 *g* for 1 minute, and the pellet was resuspended in 300 μl of 1 mM sodium deoxycholate (SDC). After gentle pipetting, samples were incubated at room temperature for 5 minutes to induce lysis. The axonemes released in the lysate were vortexed at 3,000 rpm for 1 minute using a MIX-25P vortex mixer (MIULAB, China), then centrifuged at 300 *g* for 5 minutes. The flocculent pellet containing axonemes was ready for U-ExM analysis.

Sequence alignment

The protein sequences of Calcifer orthologs from *Plasmodium yoelii*, *Plasmodium berghei*, *Plasmodium falciparum*, and *Plasmodium vivax* were retrieved from PlasmoDB: PY17X_1323900, PBANKA_1320100, PF3D7_1456400, PVP01_1250500databasehttps://plasmodb.org/. Multiple sequence alignment was performed using the MUSCLE algorithm implemented in MEGA11 software. The resulting alignment was exported in FASTA format and imported into BioEdit software (version 7.2.5) for graphical visualization. Conserved and similar amino acid residues were highlighted by background shading, with the identity and similarity threshold set at 50% (Figure S1).

QUANTIFICATION AND STATISTICAL ANALYSIS

Statistical analysis was performed using Graphpad Prism 8.0.2. Data collected as raw values are shown as mean±SEM. Details of statistical methods are reported in the figure legends. The 3D surface topology reconstruction of Z-stack images was generated using Imaris 10.2.0 software.

Current Biology, Volume *36*

Supplemental Information

Mechanoregulation of basal body integrity during *Plasmodium* exflagellation

Jiepeng Guan, Yujiao Gong, Wenqi Liang, Huiting Cui, and Jing Yuan

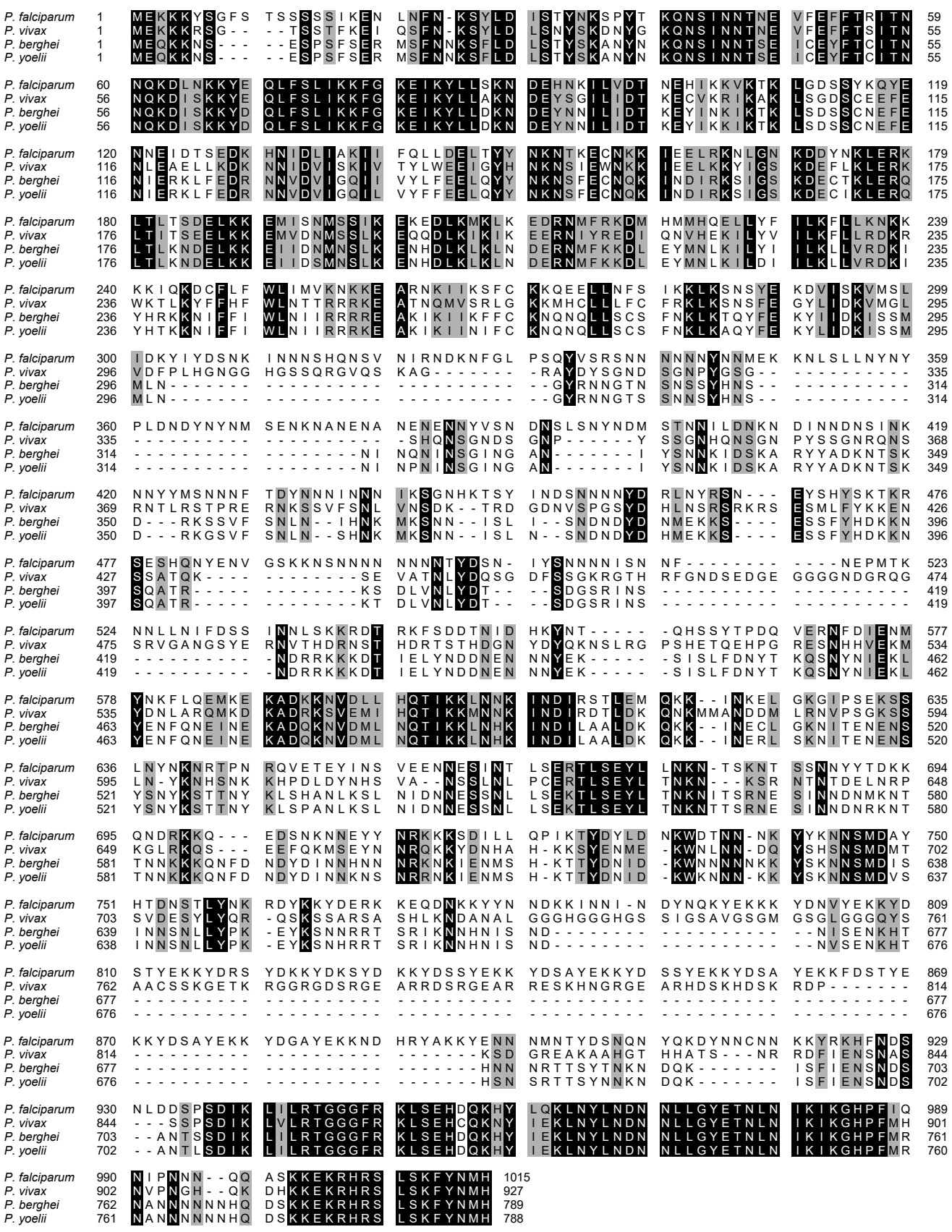

Figure S1. Protein sequence alignment of Calcifer orthologs across *Plasmodium* species. Related to STAR Methods.

Alignment of Calcifer amino acid sequences from *P. falciparum* (PF3D7_1456400), *P. vivax* (PVP01_1250500), *P. berghei* (PBANKA_1320100), and *P. yoelii* (PY17X_1323900). Identical amino acids are highlighted in black, and similar amino acids are highlighted in grey.

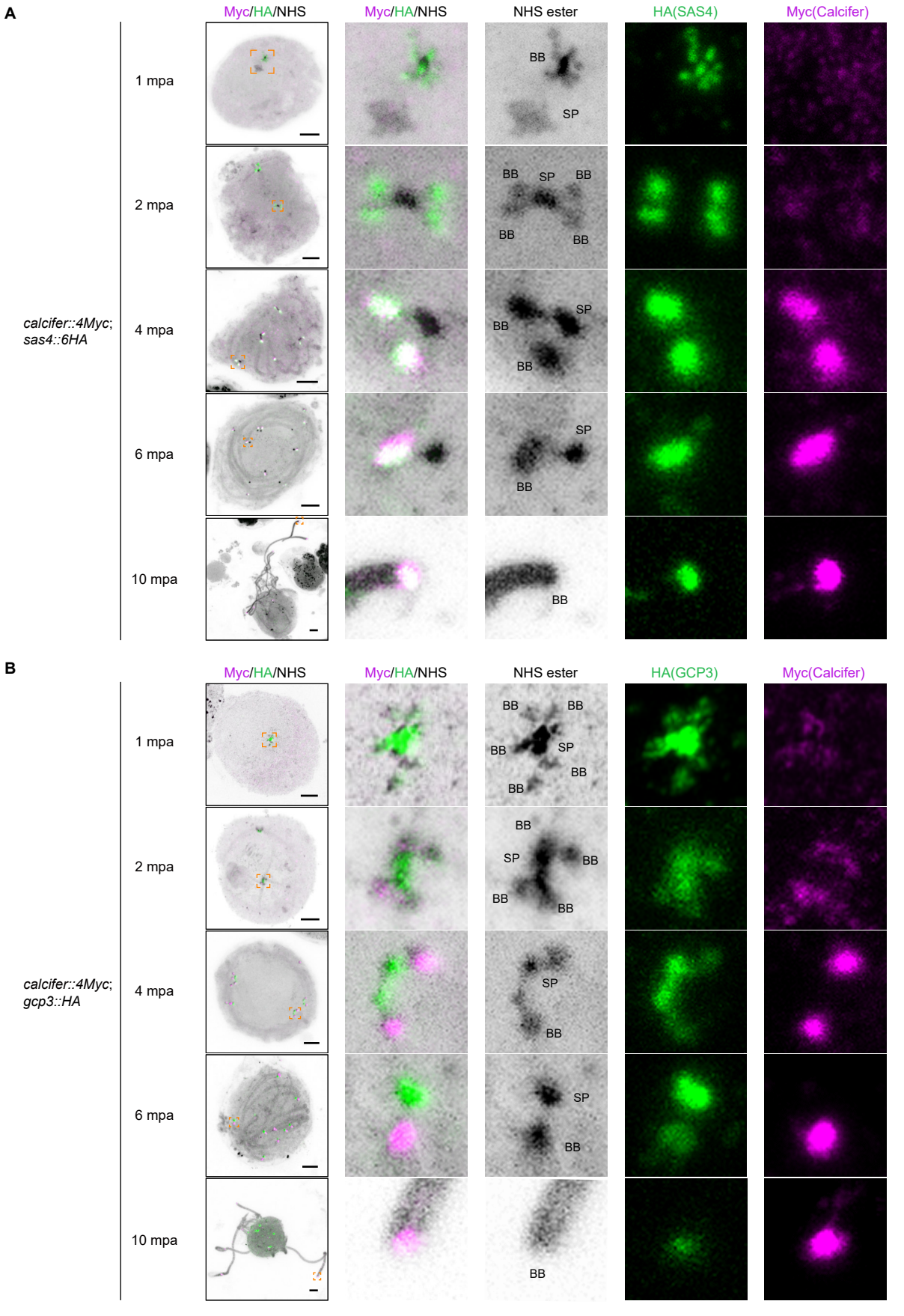
A
Myc/HA/NHS
Myc/HA/NHS
NHS ester
HA(SAS4)
Myc(Calcifer)
1 mpa
2 mpa
4 mpa
6 mpa
10 mpa
calcifer::4Myc;
sas4::6HA
BB
SP
B
Myc/HA/NHS
Myc/HA/NHS
NHS ester
HA(GCP3)
Myc(Calcifer)
1 mpa
2 mpa
4 mpa
6 mpa
10 mpa
calcifer::4Myc;
gcp3::HA
BB
SP

Figure S2. Relative spatiotemporal localization between Calcifer and two basal body proteins SAS4 and GCP3 during male gametogenesis. Related to Figure 2.
(A-B) U-ExM of male gametocytes in the double-tagged parasite lines *calcifer::4Myc*;*sas4::6HA* (A) and *calcifer::4Myc*;*gcp3::HA* (B) at the indicated time points post-activation (mpa). Magnified views of the boxed regions are shown in the right panels. SP, spindle pole; BB, basal body. Scale bars: 5 μm. Representative of three independent experiments.

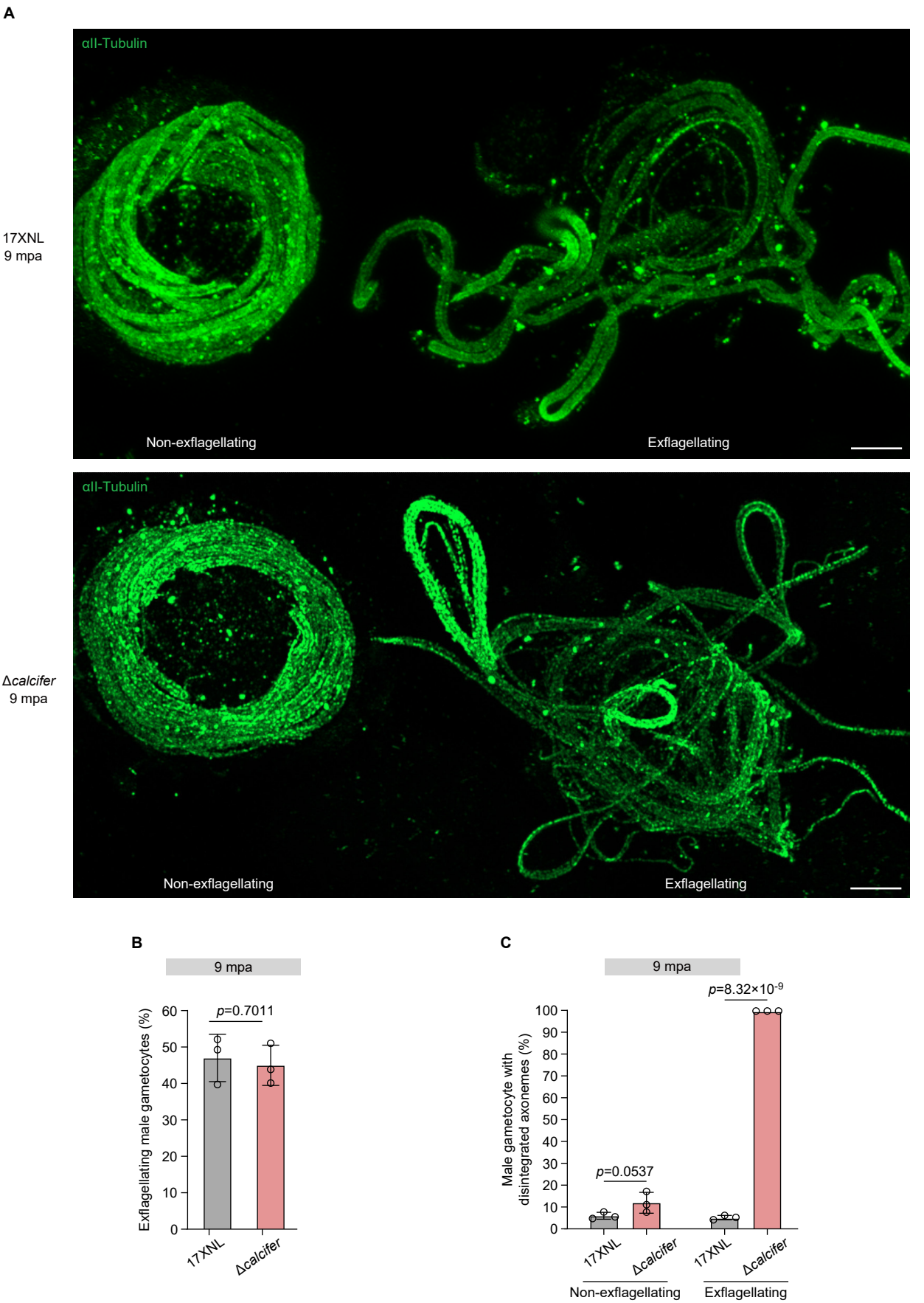
A
αII-Tubulin
17XNL
9 mpa
Non-exflagellating
Exflagellating
αII-Tubulin
Δcalcifer
9 mpa
Non-exflagellating
Exflagellating
B
9 mpa
p=0.7011
Exflagellating male gametocytes (%)
60
50
40
30
20
10
0
17XNL
Δcalcifer
C
9 mpa
p=8.32×10-9
Male gametocyte with disintegrated axonemes (%)
100
90
80
70
60
50
40
30
20
10
0
p=0.0537
17XNL
Δcalcifer
17XNL
Δcalcifer
Non-exflagellating
Exflagellating

Figure S3. Axoneme disintegrates specifically during exflagellation in Calcifer-null parasites. Related to Figures 3 and 4.

(A) U-ExM of αII-Tubulin in axoneme pre-release (non-exflagellating) and release (exflagellating) male gametocytes at 9 mpa for 17XNL and Δ*calcifer* parasites. Scale bars: 5 μm. Three independent experiments.

(B) Quantification of axoneme initial release for the parasites in A. Mean ± SEM from three independent experiments; two-sided *t*-test.

(C) Quantification of male gametocytes with disintegrated axonemes in A. Mean ± SEM from three independent experiments; two-sided *t*-test.

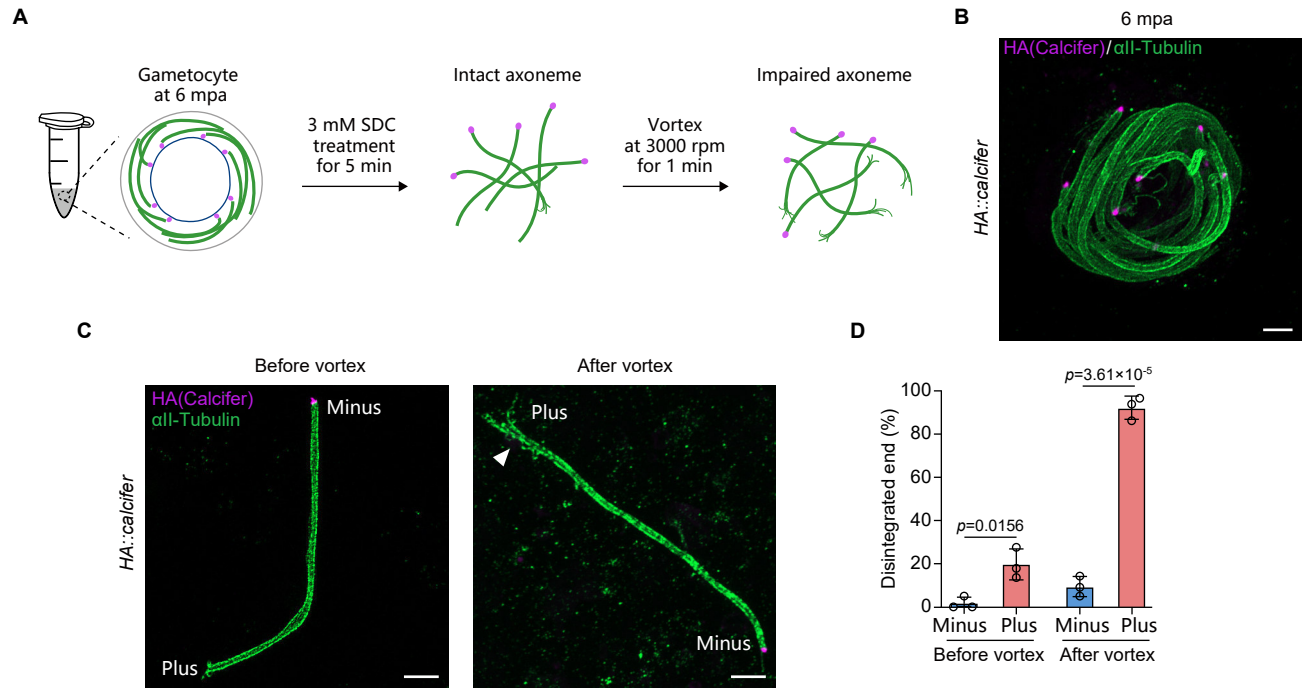
A
Gametocyte
at 6 mpa
3 mM SDC
treatment
for 5 min
Intact axoneme
Vortex
at 3000 rpm
for 1 min
Impaired axoneme
B
6 mpa
HA(Calcifer)/αII-Tubulin
HA::calcifer
C
Before vortex
After vortex
HA(Calcifer)
αII-Tubulin
HA::calcifer
Minus
Plus
Plus
Minus
D
p=3.61×10-5
p=0.0156
Disintegrated end (%)
100
80
60
40
20
0
Minus
Plus
Minus
Plus
Before vortex
After vortex

Figure S4. The basal body at axoneme minus end exhibits superior structural stability under mechanical stress generated by *in vitro* vortex. Related to Figure 5.
(A) Schematic of the *in vitro* axoneme vortex assay simulating vibration-induced mechanical stress. Axonemes released from 6 mpa male gametocytes via SDC lysis are applied to mechanical shear (3000 rpm vortex). Basal body proteins are shown in purple, and axonemes are shown in green.
(B) U-ExM of axonemes in the *HA::calcifer* male gametocytes at 6 mpa. HA-tagged Calcifer (magenta) marks the basal body at the axoneme minus end. Scale bars: 5 μm. Two independent experiments.
(C) U-ExM of isolated axonemes from the *HA::calcifer* male gametocytes before and after vortex. HA-tagged Calcifer (magenta) marks the basal body at the axoneme minus end. After vortex, most of axonemes showed intact minus ends and branched plus ends (white arrowhead). Scale bars: 5 μm. Three independent experiments.
(D) Quantification of axonemes showing disintegrated minus and plus ends in C. Mean ± SEM from three independent experiments; two-sided *t*-test.

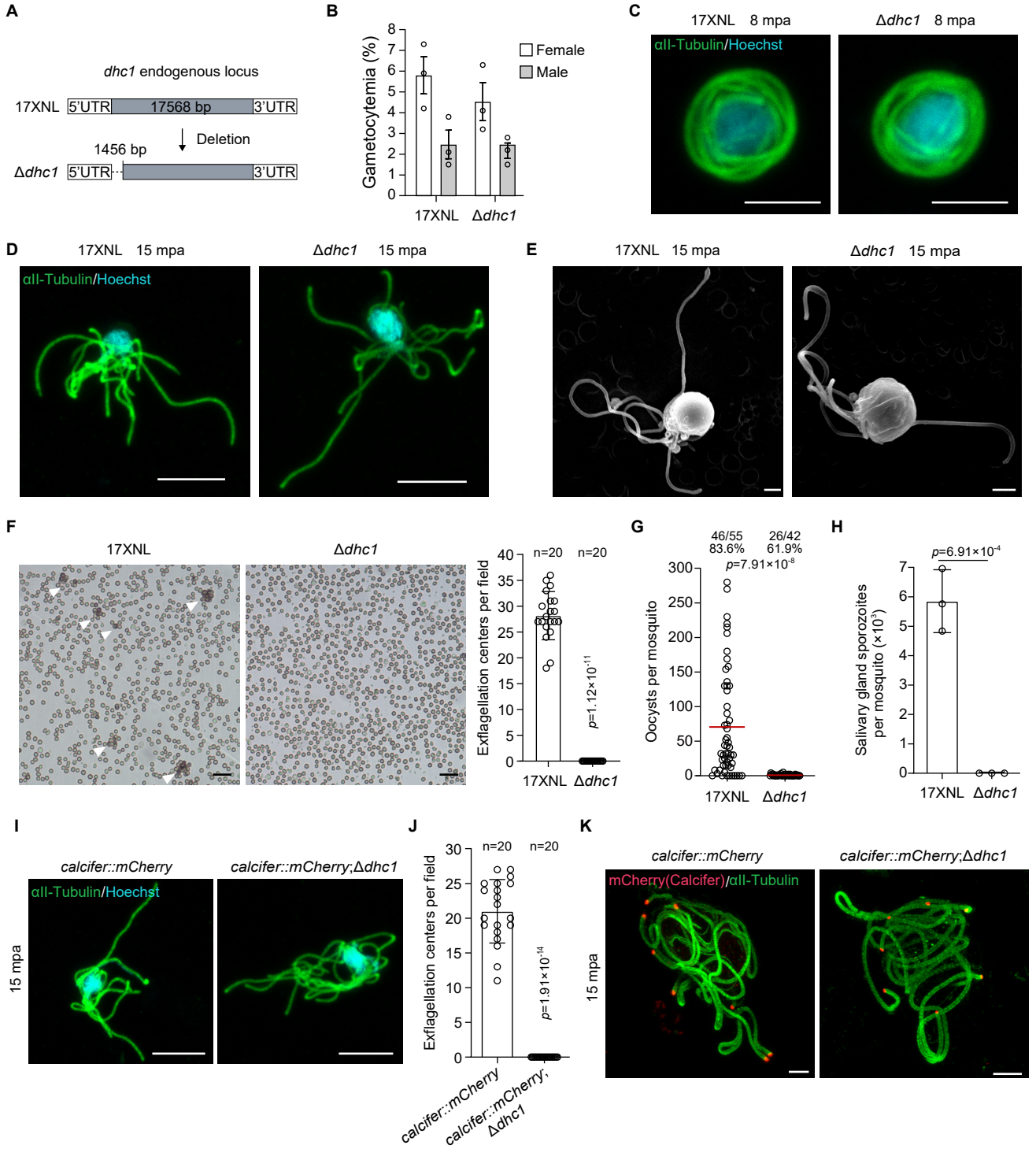
A
dhc1 endogenous locus
17XNL
5'UTR
17568 bp
3'UTR
Deletion
1456 bp
Δdhc1
5'UTR
3'UTR
B
Gametocytemia (%)
Female
Male
17XNL
Δdhc1
C
17XNL 8 mpa
Δdhc1 8 mpa
αII-Tubulin/Hoechst
D
17XNL 15 mpa
Δdhc1 15 mpa
αII-Tubulin/Hoechst
E
17XNL 15 mpa
Δdhc1 15 mpa
F
17XNL
Δdhc1
Exflagellation centers per field
n=20
n=20
p=1.12×10-11
17XNL
Δdhc1
G
46/55
83.6%
26/42
61.9%
p=7.91×10-8
Oocysts per mosquito
17XNL
Δdhc1
H
p=6.91×10-4
Salivary gland sporozoites per mosquito (×10³)
17XNL
Δdhc1
I
calcifer::mCherry
calcifer::mCherry;Δdhc1
αII-Tubulin/Hoechst
15 mpa
J
Exflagellation centers per field
n=20
n=20
p=1.91×10-14
calcifer::mCherry
calcifer::mCherry;Δdhc1
K
calcifer::mCherry
calcifer::mCherry;Δdhc1
mCherry(Calcifer)/αII-Tubulin
15 mpa

Figure S5. Dhc1 is critical for axoneme beating after initial release during male gametogenesis. Related to Figure 6 and Videos S5-6.

(A) Schematic of the *dhc1* gene deletion in *P. yoelii*. The N-terminal coding sequence (1456 bp) was deleted in the 17XNL strain, generating the mutant line Δ*dhc1*.

(B) Male and female gametocyte formation in mice. Mean ± SEM from three mice in each group. A representative from two independent experiments.

(C-D) IFA of αII-Tubulin in male gametocytes at 8 mpa (C) and 15 mpa (D). Scale bars: 5 μm. Representative of three independent experiments.

(E) Scanning electron microscopy (SEM) of exflagellating male gametocytes at 15 mpa. Scale bars: 1 μm. Three independent experiments.

(F) Exflagellation center (EC) formation of male gametocytes at 10 mpa. White arrowheads indicate ECs. Scale bars: 20 μm. Right panel: EC counts per field (n). Mean ± SEM from three independent experiments; two-sided *t*-test.

(G) Midgut oocyst formation in mosquitoes at day 7 post blood feeding. Numbers at the top indicate the ratio of infected/total mosquitoes (x/y) and the infection prevalence (%). Red lines: mean values; two-sided *t*-test. Three independent experiments.

(H) Salivary gland sporozoite formation in mosquitoes at day 14 post-blood feeding. 20 infected mosquitoes were analyzed per group. Mean ± SEM from three independent experiments; two-sided *t*-test.

(I) IFA of αII-Tubulin in the exflagellating male gametocytes at 15 mpa for the *calcifer::mCherry* and *calcifer::mCherry*;Δ*dhc1* parasites. Scale bars: 5 μm. Three independent experiments.

(J) Quantification of Exflagellation center (EC) formation in *calcifer::mCherry* and *calcifer::mCherry*;Δ*dhc1*. Mean ± SEM from three independent experiments; two-sided *t*-test.

(K) U-ExM of αII-Tubulin and mCherry in the exflagellating male gametocytes at 15 mpa for the *calcifer::mCherry* and *calcifer::mCherry*;Δ*dhc1* parasites. Scale bars: 5 μm. Three independent experiments.

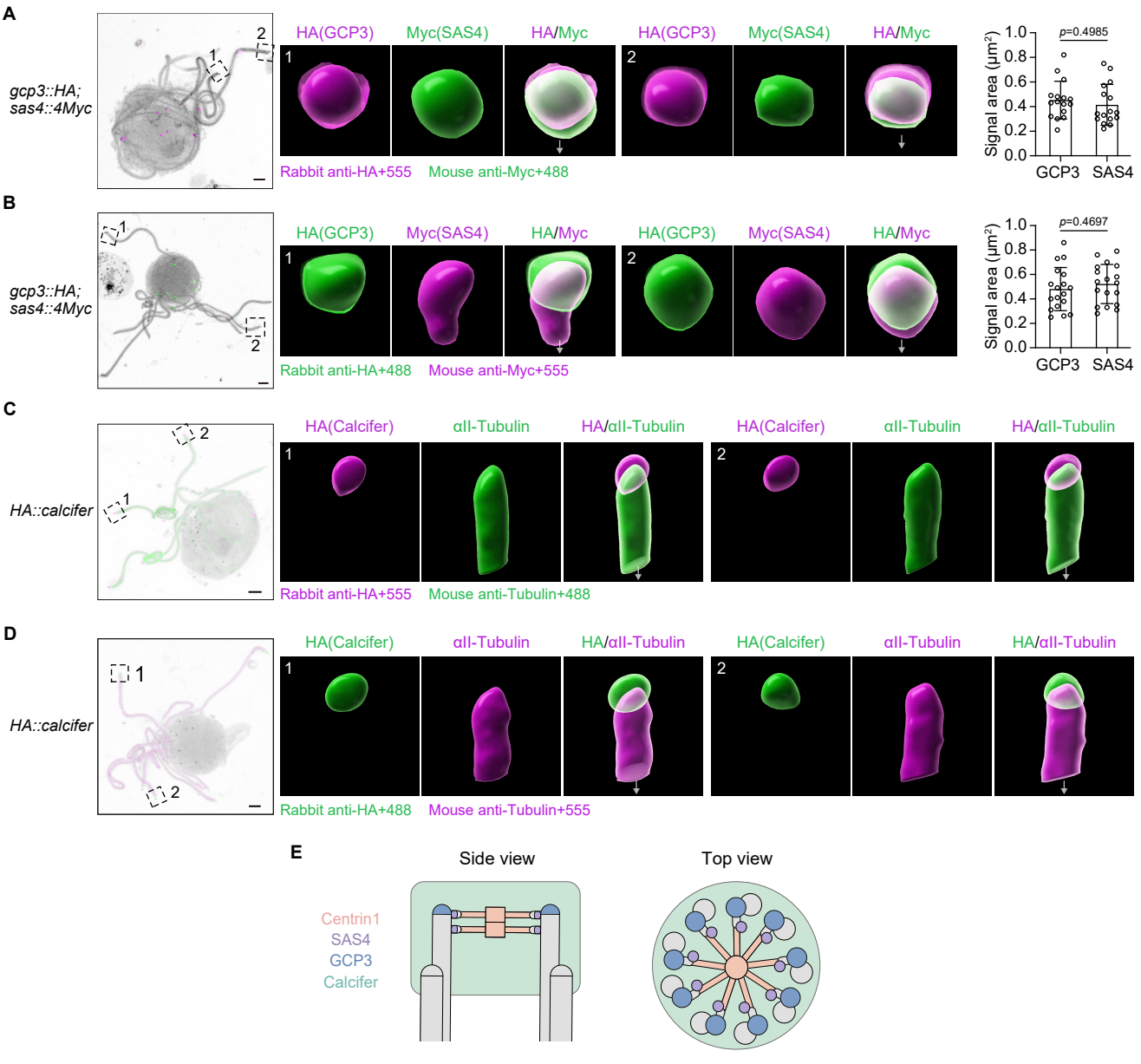
A
gcp3::HA;
sas4::4Myc
HA(GCP3)
Myc(SAS4)
HA/Myc
Rabbit anti-HA+555
Mouse anti-Myc+488
Signal area (μm²)
p=0.4985
GCP3
SAS4
B
gcp3::HA;
sas4::4Myc
Rabbit anti-HA+488
Mouse anti-Myc+555
p=0.4697
C
HA::calcifer
HA(Calcifer)
αII-Tubulin
HA/αII-Tubulin
Rabbit anti-HA+555
Mouse anti-Tubulin+488
D
HA::calcifer
Rabbit anti-HA+488
Mouse anti-Tubulin+555
E
Side view
Top view
Centrin1
SAS4
GCP3
Calcifer

Figure S6. Relative localization between SAS4 and GCP3, and between Calcifer and the axoneme. Related to Figure 7.

(A) U-ExM validation of relative spatial localization between GCP3 and SAS4 within the basal body. Left: 2D projection images of the *gcp3::HA*;*sas4::4Myc* male gametocytes at 10 mpa stained with the indicated antibodies and NHS ester. Scale bars: 5 μm. Middle: 3D surface topology reconstruction. Two boxed areas were zoomed in. White arrows show the axoneme direction. Right: Quantification of fluorescence signal area for proteins. Mean ± SEM from three independent experiments; two-sided *t*-test.

(B) Validation of relative localization between GCP3 and SAS4 by swapping fluorescent secondary antibodies. Scale bars: 5 μm.

(C) U-ExM of relative spatial localization between Calcifer and axonemal microtubule at the minus ends in the *HA::calcifer* male gametocytes at 10 mpa. Scale bars: 5 μm. Three independent experiments.

(D) Validation of relative spatial localization between Calcifer and axonemal microtubule at the minus ends by swapping fluorescent secondary antibodies. Scale bars: 5 μm. Three independent experiments.

(E) Proposed schematic model showing Calcifer localization relative to the basal body structure at the minus end of the axoneme. Side (left panel) and top views (right panel) show that Calcifer (green) forms a wrapping structure surrounding or enclosing the basal body. Centrin1, SAS4, and GCP3 are the conserved basal body component proteins. Note that *Plasmodium* exhibits a microtubule singlet-to-doublet transition for the axonemal MT doublet assembly, distinct from the canonical microtubule triplet-to-doublet transition.

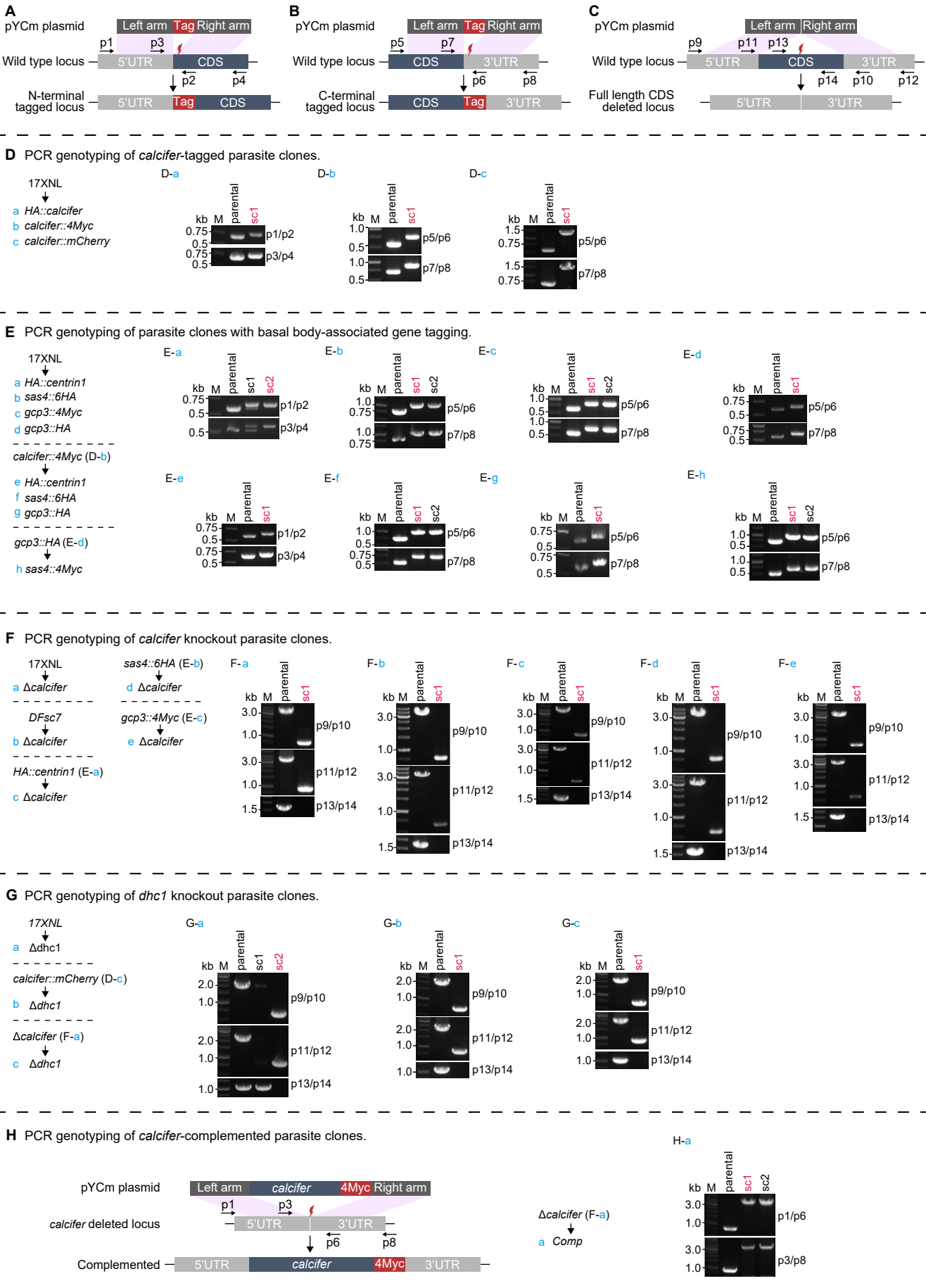
A
pYCm plasmid
Left arm
Tag
Right arm
p1
p3
Wild type locus
5'UTR
CDS
p2
p4
N-terminal tagged locus
B
pYCm plasmid
Left arm
Tag
Right arm
p5
p7
Wild type locus
CDS
3'UTR
p6
p8
C-terminal tagged locus
C
pYCm plasmid
Left arm
Right arm
p9
p11
p13
Wild type locus
5'UTR
CDS
3'UTR
p14
p10
p12
Full length CDS deleted locus
D Genotyping of calcifer-tagged parasite clones.
17XNL
a HA::calcifer
b calcifer::4Myc
c calcifer::mCherry
D-a
D-b
D-c
kb M parental sc1
p1/p2
p3/p4
p5/p6
p7/p8
E Genotyping of parasite clones with basal body-associated gene tagging.
17XNL
a HA::centrin1
b sas4::6HA
c gcp3::4Myc
d gcp3::HA
calcifer::4Myc (D-b)
e HA::centrin1
f sas4::6HA
g gcp3::HA
gcp3::HA (E-d)
h sas4::4Myc
E-a
E-b
E-c
E-d
E-e
E-f
E-g
E-h
kb M parental sc1 sc2
p1/p2
p3/p4
p5/p6
p7/p8
F Genotyping of calcifer knockout parasite clones.
17XNL
a Δcalcifer
DFsc7
b Δcalcifer
HA::centrin1 (E-a)
c Δcalcifer
sas4::6HA (E-b)
d Δcalcifer
gcp3::4Myc (E-c)
e Δcalcifer
F-a
F-b
F-c
F-d
F-e
kb M parental sc1
p9/p10
p11/p12
p13/p14
G Genotyping of dhc1 knockout parasite clones.
17XNL
a Δdhc1
calcifer::mCherry (D-c)
b Δdhc1
Δcalcifer (F-a)
c Δdhc1
G-a
G-b
G-c
kb M parental sc1 sc2
p9/p10
p11/p12
p13/p14
H Genotyping of calcifer-complemented parasite clones.
pYCm plasmid
Left arm
calcifer
4Myc
Right arm
p1
p3
calcifer deleted locus
5'UTR
3'UTR
p6
p8
Complemented
Δcalcifer (F-a)
a Comp
H-a
kb M parental sc1 sc2
p1/p6
p3/p8

Figure S7. Generation and genotyping of transgenic parasite lines. Related to STAR Methods.

(A-C) Schematics of CRISPR/Cas9-mediated gene N-terminal tagging (A), C-terminal tagging (B), and gene deletion (C) via double cross-over homologous recombination. Black arrows indicate the position of primers (p) used for parasite genotyping; red bolts indicate the sites recognized by sgRNA.

(D-G) Genotyping PCR results showing correct 5' and 3' homologous recombination in the modified parasite lines with tagging in Calcifer (D), with tagging in the basal body protein (E), with gene deletion in *calcifer* (F), and with gene deletion in *dhc1* (G). Red labels indicate the parasite clones for further analysis. All the modified parasite lines generated in this study are listed in Table S1.

(H) Schematic (left) and PCR validation (right) of the *calcifer* complemented line *Comp*. Primers and sgRNA are shown. DNA sequence of all primers and sgRNA used in this study are provided in Table S2.

Strain	Parental strain	Description	Resource
17XNL	/	*Plasmodium yoelii* 17XNL strain	NIH
Parasites with gene tagging			
DFsc7	17XNL	*DFsc7* expresses mCherry and GFP reporters mutual-exclusively in the female and male gametocytes	Yuan lab[S1]
HA::calcifer	17XNL	Calcifer N-terminally tagged with HA	In this study
calcifer::4Myc	17XNL	Calcifer C-terminally tagged with 4Myc	In this study
calcifer::mCherry	17XNL	Calcifer C-terminally tagged with mCherry	In this study
HA::centrin1	17XNL	Centrin1 N-terminally tagged with HA	In this study
calcifer::4Myc ;*HA::centrin1*	*calcifer::4Myc*	Centrin1 N-terminally tagged with HA	In this study
sas4::6HA	17XNL	SAS4 C-terminally tagged with 6HA	In this study
calcifer::4Myc;sas4::6HA	*calcifer::4Myc*	SAS4 C-terminally tagged with 6HA	In this study
calcifer::4Myc;gcp3::HA	*calcifer::4Myc*	GCP3 C-terminally tagged with HA	In this study
gcp3::4Myc	17XNL	GCP3 C-terminally tagged with 4Myc	In this study
gcp3::HA	17XNL	GCP3 C-terminally tagged with HA	In this study
gcp3::HA;sas4::4Myc	*gcp3::HA*	SAS4 C-terminally tagged with 4Myc	In this study
Parasites with gene knockout			
Δ*calcifer*	17XNL	Deletion of the whole coding sequences of c*alcifer*	In this study
Δ*calcifer*	*DFsc7*	Deletion of the whole coding sequences of *calcifer*	In this study
Δ*nek4*	17XNL	Deletion of the partial coding sequences of *nek4*	Yuan lab[S2]
Δ*map2*	17XNL	Deletion of the partial coding sequences of *map2*	Yuan lab[S2]
HA::centrin1 ;Δ*calcifer*	*HA::centrin1*	Deletion of the whole coding sequences of *calcifer*	In this study
sas4::6HA ;Δ*calcifer*	*sas4::6HA*	Deletion of the whole coding sequences of *calcifer*	In this study
gcp3::4Myc ;Δ*calcifer*	*gcp3::4Myc*	Deletion of the whole coding sequences of *calcifer*	In this study
Δ*dhc1*	17XNL	Deletion of the N-terminal 1456 bp coding sequence of *dhc1*	In this study
calcifer::mCherry ;Δ*dhc1*	*calcifer::mCherry*	Deletion of the N-terminal 1456 bp coding sequence of *dhc1*	In this study
Δ*calcifer;* Δ*dhc1*	Δ*calcifer*	Deletion of the N-terminal 1456 bp coding sequence of *dhc1*	In this study
Parasites with gene complementation			
Comp	Δ*calcifer*	*In situ* complementation of *calcifer* C-terminally tagged with 4Myc	In this study

Table S1. List of genetically modified parasite lines in this study. Related to STAR Methods.

Oligo sequences for constructing gene tagging plasmids								
Gene name	Gene ID	Tag	Left homologous arm		Right homologous arm		Target site of sgRNA	
			Forward primer	Reverse primer	Forward primer	Reverse primer	Forward oligo	Reverse oligo
calcifer	PY17X_1323900	N-terminal HA	CCCAAGCTTGGCATTACTGTCGAAGGACT	CATGCCATGGATTAATTACAAGGAAAGGTA	CCGCTCGAGATGGAACAAAAAAAAATAG	CCCCTTAAGACCTGTTTATCAAAATGCGA	TATTGTAAATATGAAGGGAGGAGGA	AAACTCCTCCTCCCTTCATATTTAC
calcifer	PY17X_1323900	C-terminal 4Myc	CGGGGTACCCAATTCTATGGATGTATCAA	CATGCCATGGATGCATGTTATAAAACTTAG	CCGCTCGAGAAATATACTAAAATTTATAC	CCCCTTAAGCCATAGAACCAATTGCATTA	TATTGCGTTATCGTTACTAATATTG	AAACCAATATTAGTAACGATAACGC
calcifer	PY17X_1326000	C-terminal mCherry	CGGGGTACCCAATTCTATGGATGTATCAA	CATGCCATGGATGCATGTTATAAAACTTAG	CCGCTCGAGAAATATACTAAAATTTATAC	CCCCTTAAGCCATAGAACCAATTGCATTA	TATTGCGTTATCGTTACTAATATTG	AAACCAATATTAGTAACGATAACGC
centrin1	PY17X_0207700	N-terminal HA	CCCAAGCTTGGCTTGACATTTAACAAGCG	CATGCCATGGTTTAATTAATCTCAATTAAAATACG	CCGCTCGAGATGAATAGAAAAAATCAAAATATG	CCGCTTAAGGTTTATACATGCACATAATTG	TATTGTTTGTTTGATATTACACCTG	AAACCAGGTGTAATATCAAACAAAC
sas4	PY17X_1326000	C-terminal 6HA	CGGGGTACCCATGCTTGTTCCTCAATTCA	CATGCCATGGATTTAACCTTTTTATGACACCT	CCGGAATTCAACACTAAATATAATTAACAAATATTCTCG	CCCCTTAAGCCAAACAATGGCTAACAATT	TATTGTTTCTTTCGAGATTTCCTAA	AAACTTAGGAAATCTCGAAAGAAAC
sas4	PY17X_1326000	C-terminal 4Myc	CGGGGTACCCATGCTTGTTCCTCAATTCA	CATGCCATGGATTTAACCTTTTTATGACACCT	CCGGAATTCAACACTAAATATAATTAACAAATATTCTCG	CCCCTTAAGCCAAACAATGGCTAACAATT	TATTGTTTCTTTCGAGATTTCCTAA	AAACTTAGGAAATCTCGAAAGAAAC
gcp3	PY17X_0837700	C-terminal HA	CGGGGTACCTCTCACATGATAATGGAAATGATG	CATGCCATGGTTTGCTTATCATGTTTATTTGCTTG	CCGCTCGAGGCATGATAAGCAAATAACTCG	CCCCTTAAGAAATCGTTCTGTATGCTCACT	TATTCTCGGTGTCAGGGCGAGTTT	AAACAAACTCGCCCTGACACCGAG
gcp3	PY17X_0837700	C-terminal 4Myc	CGGGGTACCTCTCACATGATAATGGAAATGATG	CATGCCATGGTTTGCTTATCATGTTTATTTGCTTG	CCGCTCGAGGCATGATAAGCAAATAACTCG	CCCCTTAAGAAATCGTTCTGTATGCTCACT	TATTCTCGGTGTCAGGGCGAGTTT	AAACAAACTCGCCCTGACACCGAG
Diagnositc PCR primers for N-terminal tagging								
Gene name	**Gene ID**	**Tag**	**P1**	**P2**	**P3**	**P4**		
calcifer	PY17X_1323900	N-terminal HA	GGGGGGAATGATGGAAAAAA	ACTAAATGAAGGCGACTCAC	GTTCTTTTACCTTTCCTTGT	GGAAAGGTTTTGTGTAGCTA		
centrin1	PY17X_0207700	N-terminal HA	GTGATATCTTCGATTTAATTT	GCGCTTCTTATCATATTTTG	GTCACCACCATATTATCATATC	GTATAACTATGGTTTTATAG		
Diagnositc PCR primers for C-terminal tagging								
Gene name	**Gene ID**	**Tag**	**P5**	**P6**	**P7**	**P8**		
calcifer	PY17X_1323900	C-terminal 4Myc	CTCATAAAACCACGTATGAT	AGAGATTTCCTTCTGAATTG	CATCAAGACAGCAAAAAGGA	AACGTCTTTTCCTTCGTCCC		
calcifer	PY17X_1323900	C-terminal mCherry	CTCATAAAACCACGTATGAT	AGAGATTTCCTTCTGAATTG	CATCAAGACAGCAAAAAGGA	AACGTCTTTTCCTTCGTCCC		
sas4	PY17X_1326000	C-terminal 6HA	CTTCCCTAATTCGTATACGG	CTCTCCAACTTAAAAATGAAGG	GGTTGTAGGTGTCATAAAAAGG	ATATTTACGGCCATTCTACG		
sas4	PY17X_1326000	C-terminal 4Myc	CTTCCCTAATTCGTATACGG	CTCTCCAACTTAAAAATGAAGG	GGTTGTAGGTGTCATAAAAAGG	ATATTTACGGCCATTCTACG		
gcp3	PY17X_0837700	C-terminal HA	TACTACATATTCTTCCCCAA	GAGTTATTTGCTTATCATGC	AGCAAATAAACATGATAAGC	TGTAGTGTTTCAATTCTTCA		
gcp3	PY17X_0837700	C-terminal 4Myc	TACTACATATTCTTCCCCAA	GAGTTATTTGCTTATCATGC	AGCAAATAAACATGATAAGC	TGTAGTGTTTCAATTCTTCA		
Oligo sequences for constructing gene knockout plasmids								
Gene name	**Gene ID**	**Gene size (bp) / deleted gene size (bp)**	**Left homologous arm**		**Right homologous arm**		**Target site of sgRNA**	
			Forward primer	**Reverse primer**	**Forward primer**	**Reverse primer**	**Forward oligo**	**Reverse oligo**
calcifer	PY17X_1323900	2689/2689	CGGGGTACCGTGTGTATAGGCACGCTATT	CATGCCATGGATTAATTACAAGGAAAGGTA	CCGCTCGAGAAATATACTAAAATTTATAC	CCCCTTAAGCCATAGAACCAATTGCATTA	TATTGTAATGCGTAGACAACATTAT	AAACATAATGTTGTCTACGCATTAC
dhc1	PY17X_0418900	17568/1456	CGGGGTACCGAAATGAATGAGAATATGCG	CATGCCATGGTTTTTTATCATTTGGATAAT	CCGCTCGAGATGATTCTGATGAAGAAGTG	CCGGAATTCCGTTCTTGTAAATCACTTTC	TATTGTAAATTGTTAAGTTTATTCG	AAACCGAATAAACTTAACAATTTAC
Diagnostic PCR primers for gene knockout								
Gene name	**Gene ID**	**P9**	**P10**	**P11**	**P12**	**P13**	**P14**	
calcifer	PY17X_1323900	GCAAAAAGGGGGGAATGATG	CATTTGGGAAAATTGAACAG	GTTCTTTTACCTTTCCTTGT	AACGTCTTTTCCTTCGTCCC	CACAAAACCTTTCCATTTTT	ATTCCTTTGGGTACAACAAG	
dhc1	PY17X_0418900	GAAGCAGTTTGAATCGTTTC	CCACTTCTTCATCAGAATCAT	GATGCATGTACATATGAATAGG	GTAAAATATCATATGTTGTGTG	AAAATGACGAAGTAGATGTT	AATTGTTAAGTTTATTCGGGG	
Oligo sequences for constructing gene *in situ* complementation plasmids								
Strain	**Gene ID**	**Tag**	**Left homologous arm**		**Right homologous arm**		**Target site of sgRNA**	
			Forward primer	**Reverse primer**	**Forward primer**	**Reverse primer**	**Forward oligo**	**Reverse oligo**
Comp	PY17X_1323900	C-terminal 4Myc	CGGGGTACCGGCATTACTGTCGAAGGACT	CATGCCATGGATGCATGTTATAAAACTTAG	CCGCTCGAGAAATATACTAAAATTTATACAATTCAGAAG	CCCCTTAAGCCATAGAACCAATTGCATTA	TATTGCGGACGCTAATCGTAGCTA	AAACTAGCTACGATTAGCGTCCGC
Diagnostic PCR primers for *in situ* complementation gene								
Strain	**Gene ID**	**Tag**	**P1**	**P6**	**P3**	**P8**		
Comp	PY17X_1323900	C-terminal 4Myc	GGGGGGAATGATGGAAAAAA	AGAGATTTCCTTCTGAATTG	GTTCTTTTACCTTTCCTTGT	AACGTCTTTTCCTTCGTCCC		
Note: The blue sequences are designed for the restriction enzyme digestion.								

Table S2. Oligonucleotides and primers used in this study. Related to STAR Methods.

Supplemental References

S1. Liu, C., Li, Z., Jiang, Y., Cui, H., and Yuan, J. (2018). Generation of *Plasmodium yoelii* malaria parasite carrying double fluorescence reporters in gametocytes. Mol Biochem Parasitol *224*, 37-43. 10.1016/j.molbiopara.2018.07.010.

S2. Jiang, Y., Wei, J., Cui, H., Liu, C., Zhi, Y., Jiang, Z., Li, Z., Li, S., Yang, Z., Wang, X., et al. (2020). An intracellular membrane protein GEP1 regulates xanthurenic acid induced gametogenesis of malaria parasites. Nat Commun *11*, 1764. 10.1038/s41467-020-15479-3.